Climate Dynamics

The European Russia Drought Atlas

--Manuscript Draft--

Manuscript Number:	
Full Title:	The European Russia Drought Atlas
Article Type:	Original Article
Keywords:	European Russia; East European Plain; Drought Atlas; Tree-ring network; Droughts and Heat Waves
Corresponding Author:	Edward R. Cook Lamont-Doherty Earth Observatory UNITED STATES
Corresponding Author Secondary Information:	
Corresponding Author's Institution:	Lamont-Doherty Earth Observatory
Corresponding Author's Secondary Institution:	
First Author:	Edward R. Cook
First Author Secondary Information:	
Order of Authors:	Edward R. Cook
	Olga Solomina
	Vladimir Matskovsky
	Benjamin I. Cook
	Leonid Agafonov
	Alina Berdnikova
	Ekaterina Dolgova
	Aleksey Karpukhin
	Natallia Knysh
	Marina Kulakova
	Veronika Kuznetsova
	Tomáš Kyncl
	Josef Kyncl
	Olga Maximova
	Irina Panyushkina
	Andrea Seim
	Denis Tishin
	Tomasz Ważny
	Maxim Yermokhin
Order of Authors Secondary Information:	
Funding Information:	
Abstract:	We present the European Russia Drought Atlas (ERDA) covering the East European Plain to the Ural Mountains. Like the Old World Drought Atlas (OWDA) for the Euro-Mediterranean region, the ERDA is a one-half degree gridded reconstruction of

	summer Palmer Drought Severity Indices estimated from a network of annual tree-ring chronologies. Ensemble point-by-point regression is used to generate the ERDA with the identical protocols used for developing the OWDA. Split calibration/validation tests of the ERDA indicate that it has significant skill over most of its domain and is much more ¬¬skillful than the OWDA where they overlap in the western part of ERDA domain. Comparisons to historical droughts over European Russia additionally support the ERDA's overall validity. The ERDA has been spatially smoothed and infilled using a local regression method to yield a spatially complete drought atlas back to 1400 CE. EOF analysis indicates that there are three principal modes of hydroclimatic variability in the ERDA. After Varimax rotation, these modes correlate significantly with independent climate data sets extending back to the late 19th century in a physically interpretable way and relate to atmospheric circulation dynamics of droughts and heatwaves over European Russia based on more recent instrumental data.
Suggested Reviewers:	Tim Osborn T.Osborn@uea.ac.uk Expert in physical climatology and paleoclimatology over the European sector.
	Connie Woodhouse conniew1@email.arizona.edu Expert in quantitative palaeoclimatology methods.
	Jürg Luterbacher Juerg.Luterbacher@geogr.uni-giessen.de Knowledgeable in climate dynamics and palaeoclimatology
	Siegfried Schubert siegfried.d.schubert@nasa.gov Expert in Eurasian climatology

The European Russia Drought Atlas

Edward R. Cook[1,*]
Olga Solomina[2]
Vladimir Matskovsky[3]
Benjamin I. Cook[4]
Leonid Agafonov[5]
Alina Berdnikova[6]
Ekaterina Dolgova[7]
Aleksey Karpukhin[8]
Natallia Knysh[9]
Marina Kulakova[10]
Veronika Kuznetsova[11]
Tomáš Kyncl[12]
Josef Kyncl[12]
Olga Maximova[13]
Irina Panyushkina[14]
Andrea Seim[15]
Denis Tishin[16]
Tomasz Ważny[14,17]
Maxim Yermokhin[9]

[1]Lamont-Doherty Earth Observatory of Columbia University, Palisades, NY, USA
[2]Institute of Geography, Russian Academy of Sciences (RAS), Moscow, Russia
[3]Institute of Geography, RAS, Moscow, Russia
[4]NASA Goddard Institute for Space Studies, New York, NY, USA
[5]Institute of Plant and Animal Ecology, Ekaterinburg, Russia
[6]Faculty of Geography, Moscow State University, Moscow, Russia
[7]Institute of Geography, RAS, Moscow, Russia
[8]Institute of Archaeology, RAS, Moscow, Russia
[9]Institute of Experimental Botany NASB, Minsk, Belarus
[10]Archaeological Center of Pskovskaya Oblast, Pskov, Russia
[11]Institute of Geography, RAS, Moscow, Russia
[12]DendroLab Brno, Brno 61600, Czech Republic
[13]Institute of Geography, RAS, Moscow, Russia
[14]Laboratory of Tree-Ring Research, University of Arizona, Tucson, USA
[15]Institute of Forest Sciences, University of Freiburg, Freiburg, Germany
[16]Kazan Federal University, Kazan, Russia
[17]Nicolaus Copernicus University, Torun 87-100, Poland

*Corresponding author: Tel. +1 845 365 8618
E-mail address: drdendro@ldeo.columbia.edu (E. R. Cook)

Key words:

European Russia
East European Plain
Drought Atlas
Tree-ring network
Droughts and Heat Waves

Abstract

We present a new drought atlas for the East European or Russian Plain extending from eastern Europe to the Ural Mountains: the European Russia Drought Atlas or ERDA. Like the Old World Drought Atlas (OWDA) for the Euro-Mediterranean region, the ERDA is a one-half degree gridded reconstruction of summer Palmer Drought Severity Indices estimated from a network of annual tree-ring chronologies in European Russia and surrounding countries. Ensemble point-by-point regression was used to generate the ERDA with the identical protocols used for developing the OWDA. Split calibration/validation tests of the ERDA indicate that it has significant skill over most of its domain and is more skillful than the OWDA in the western part of ERDA domain. Comparisons to historical droughts over European Russia further support the ERDA's overall validity. The ERDA has been spatially smoothed and infilled using a local regression method to yield a spatially complete drought atlas back to 1400 CE. EOF analysis indicates that there are three principal modes of hydroclimatic variability in the ERDA. After Varimax rotation, these modes correlate significantly with independent climate data sets extending back to the late 19th century in a physically interpretable way and relate to atmospheric circulation dynamics of droughts and heatwaves over European Russia based on more recent instrumental data.

1. Introduction

For many centuries, the Russian economy was fully dependent on the cereal harvests of important grain crops such as wheat, rye, and barley. Before the development of the virgin and highly fertile Black Earth or Chernozem soils for farming in Kazakhstan and southern Siberia in the 20th century, Russian agriculture was mainly concentrated in the European territories west of the Ural Mountains where most of the population was living. However, because of its high latitude location and continentality, European Russia (that part of Russia extending from its westernmost political border eastward to the Urals) was always a land of "risky agriculture" where harvest yields were often below expectation due to adverse weather conditions (Golubev and Dronin 2004; Dronin and Bellinger 2005). Crops in the more northerly lands often suffered from cold and wet summers and late frosts in the spring, while the southern and eastern "bread basket" territories of European Russia were regularly affected by severe droughts in the summer. Many of the current "bread basket" areas of Russia, including the Chernozem lands, the lower Volga region, and the southern part of Siberia, are projected to experience reductions in spring wheat yields before the end of the 21st century under multiple climate change scenarios due to an increase in aridity (Pavlova et al 2019). Similar reduced grain yield projections can be found in Kiselev et al (2013) for rain-fed crops.

Climate perturbations have always strongly affected the Russian economy and social life, as far back as medieval times (Klimenko and Solomina 2010). Droughts leading to poor crops provoked social instability and sometimes large-scale riots and revolts. Historical chronicles from monasteries starting in the beginning of the past millennium provide direct information on local and regional droughts, but they also mention "hungers", increases of grain prices, and other social phenomena indirectly connected to impacts of climatic extremes. Unfortunately, these historical records are heterogeneous in time (availability decreases back in time) and in space (records mainly from regions where monasteries are located).

Borisenkov and Pasetsky (1988) indicate that the number of recorded droughts increased from 18 in the 10th century to 70 in the 19th century. Conversely, the number of rainy summers

93 increased from 6 to 53, and the number of famines from 13 to 85, over the same time period. It
94 is not clear how much of these trends are connected to uneven historical information or are
95 reflections of changing climatic conditions. To determine so requires an independent source of
96 past hydroclimatic variability over European Russia extending back hundreds of years in the past,
97 hence the need for a high-quality tree-ring drought atlas that is specifically targeted to this
98 region.
99
100 The existing Old World Drought Atlas (OWDA) (Cook et al 2015) covering the Euro-Mediterranean
101 region appears to fill much of this information gap. However, it is not adequate for two reasons.
102 First, the eastern limit of the OWDA domain only extends half way across the East European
103 (Russian) Plain and therefore does not fully cover the grain producing areas there. Second, the
104 tree-ring network used to produce the OWDA included only ten tree-ring chronologies from
105 within the former European USSR sector: four from northwest Russia, four from western Ukraine,
106 and two from Georgia. The drought reconstructions from the Russian region of the OWDA are
107 consequently weak with low model validation skill (see Fig. S11 in the Supplementary Materials
108 of Cook et al 2015 and below). These limitations render the OWDA inadequate for investigating
109 past periods of unusual drought and wetness in European Russia.
110
111 The frequency and severity of droughts in European Russia has been studied since the mid-20th
112 century using hydrometeorological records (Rudenko 1958; Drozdov 1980; Meshcherskaya and
113 Blazhevich 1997; Cherenkova 2007, 2012; Schubert et al 2014), historical data (Bogolepov 1907,
114 1922; Buchinsky 1957; Borisenkov and Pasetsky 1988; Voronov 1992; Borisenkov and Pasetsky
115 2003), stratigraphy of lake sediments (Shostakovich 1934; Rauner 1981; Popova 2001), and tree-
116 rings (Shvedov 1892; Chernavskaya 1985; Krenke and Chernavskaya 1998; Matveev et al 2012a,
117 b; Solomina et al 2005, 2012, 2017; Matskovsky et al 2017). However, high-resolution and
118 spatially complete field reconstructions of past drought and wetness for this area have been
119 unavailable. To fill this information gap, we have developed and present herein the European
120 Russia Drought Atlas (ERDA) covering the period 1400 to 2016 CE. The ERDA is a 4,259-point field
121 reconstruction of the June-July-August (JJA) average self-calibrating Palmer Drought Severity

Index (scPDSI) (Wells et al 2004; van der Schrier et al 2013) based on a greatly improved network of 697 annual tree-ring chronologies distributed over the ERDA domain (Fig. 1). In addition, this domain now includes all of European Russia, providing a high-quality spatiotemporal reconstruction that we can use to analyze summer season drought variability in the region over the last ~600 years.

2. Regional Climate Setting

The East European Plain is located in the high-to-mid latitudes between the Arctic Ocean to the north, the Black and Caspian Seas to the south, and from the Polish/Ukraine frontier in the west to the western slope of the Urals Mountains in the east (Fig. 1). The radiation balance in winter is negative for the whole East European Plain except for the southernmost territories, while in summer it is positive everywhere. The climate is most strongly influenced by the westerlies. Air masses from the Atlantic Ocean in winter bring warmth and precipitation, while in summer they are responsible for cool and wet weather conditions. Because of increased continentality, air masses are drier as one moves east and are also warmer in summer and colder in winter (Klimenko and Solomina 2010).

Summer season droughts and heat waves over this region are typically caused by persistent anticyclones (Obukhov et al 1984; Schubert et al 2014; Stefanon et al 2012), often originating from the Arctic (Buchinsky 1976; Kleschenko 2005) and associated with quasi-stationary Rossby wave trains (Schubert et al 2011; 2014). Dry and hot conditions in European Russia are often concurrent with cool and wet conditions to the east or west, further highlighting the importance of zonal wave structures in the atmosphere for summer season climate variability in the region (Gershunov and Douville 2008). A canonical example of such a pattern was observed in the summer of 2010, when a stationary Rossby wave simultaneously caused the occurrence of extreme drought and heat in European Russia and severe precipitation and flooding in Pakistan (Lau and Kim 2011; Schubert et al. 2011). These summer circulation anomalies over European Russia arise predominately from internal atmospheric variability (Schubert et al 2014, 2016), and

may be associated with the Eastern Atlantic/Western Russia (EA/WR) and Scandinavian (SCA) patterns (Rocheva 2012).

Alisov (1969) subdivides the territory of the East European Plain into three climatic areas: 1. Northern Atlantic-Arctic area (southern boundary located between Lake Ladoga near St. Petersburg and the Pechora River in northwest Russia). 2. Middle Atlantic-continental area (southern boundary from the mid-Dniester to the mid-Volga Rivers) 3. Southern continental area. The areas are also subdivided into the western and eastern sub-areas with the boundary running from the Northern Dvina River to the mouth of the Dnieper River. The climate is mirrored by the vegetation and soil zones. The major zones contained within the East European Plain from north to south are tundra, forest-tundra, forest, forest-steppe, semi-desert and desert.

The longest instrumental records in Eastern Europe go back to the mid-18th century. Gazina and Klimenko (2008) analyzed winter, summer, and annual temperature variations of the four longest meteorological stations in Eastern Europe that have few or no gaps (St. Petersburg, Vilnius, Moscow, and Riga). For this analysis, they used the data in the databank RIHMI-WDC (http://www.meteo.ru/data/mdata.htm) as well as earlier records of Kupfer (1846), Veselovsky (1857), Vil'd (1883), and Wahlén (1886). Gazina and Klimenko (2008) found that during the last two centuries winter temperatures have increased (up to 3°C) at all four stations, while summer temperatures have decreased. These findings contrast with Western Europe, where both winter and summer warming have occurred. In general, precipitation is also much more variable than temperature between regions across the East European Plain. Annual precipitation amounts in northern (St. Petersburg) and central (Moscow) parts of the Plain are highly correlated. This is also the case for southern (Kiev and Odessa) parts of the Plain. However, differences in inter-annual variability and long-term trend in annual precipitation between the north and south are quite large. The increase in annual precipitation over the last 150 years is significant both in Moscow and St. Petersburg, but the trend is insignificant in the southern regions.

3. Data

A. Climate data sets

The self-calibrating PDSI data used here as the target field for reconstruction is based on CRU TS 3.25 gridded temperature and precipitation data (Osborn et al 2017; 0.5° resolution). It covers the period 1901-2016. See https://crudata.uea.ac.uk/cru/data/drought/ for details. Other climate data sets used here for analyses of the ERDA include Global Precipitation Climatology Centre precipitation (GPCC; Schneider et al 2018; 1.0° resolution), Berkeley Earth global temperature (BEST; Muller et al 2013; 1.0° resolution), UCAR global scPDSI (UCAR; Dai and Zhao 2017; 2.5° resolution), and upper air data from the 20th Century Reanalysis (Compo et al 2011; 2.0° resolution). These latter data sets are available for use at KNMI Climate Explorer (van Oldenborgh and Burgers 2005; http://climexp.knmi.nl/).

B. Tree-Ring Data

Figure 1 shows the distribution of tree-ring chronologies used in developing the ERDA, a total of 697 chronologies in all, many of them developed specifically for this project. Within just European Russia itself, the network has increased from only four chronologies used in the OWDA to 275 chronologies used here. This includes tree-ring series from eight species: *Pinus sylvestris* L. (156 series), *Larix sibirica* Ledeb. (39 series), *Picea obovata* Ledeb. (33 series), *Picea abies* (L.) H. Karst. (32 series), and *Quercus robur* L. (9 series), *Abies* nordmanniana (Stev.) Spach (3 series), *Fagus orientalis* Lipsky (2 series), and *Pinus halepensis* Mill. (1 series).

Recently, strong efforts have been made to sample in areas south of the taiga regions in the hotter and more droughty parts of European Russia where the tree-ring network has been historically very sparse. Matskovsky (2016) analyzed the climate sensitivity of ring widths for the most common species growing on the overall East European Plain and concluded that the region located at 55-60°N is the approximate border between temperature and drought sensitive

conifer tree species. Thus, the development of the European Russia tree-ring network south of 60°N has been especially important to this project. To this end, Solomina et al (2017) developed a relatively uniform network of 59 chronologies covering this southern region. These developments were supported by decades of research in the Povolzhie region (Askeyev et al 2005; Tishin et al 2014) and Northern Caucasus (Solomina et al 2012; Dolgova 2016). Among the noteworthy network developments has also been the creation of new chronologies from Belarus (Yermokhin and Knysh 2016; Knysh and Yermokhin 2019), where the number of tree-ring chronologies in the network increased from none to 23, mainly a mix of *P. sylvestris* and *Q. robur* series.

In addition to the chronologies lying inside the ERDA domain, chronologies surrounding this area are included to the dataset (Fig. 1). They are chronologies from Eastern and Central Europe (Cook et al 2015), from Western Siberia (Agafonov and Gurskaya 2012, 2013; Gurskaya et al 2012; Agafonov et al 2016), and the Central Asia countries of Kyrgyzstan (Graybill et al 1992; Esper et al 2003; Solomina et al 2012, 2014; Seim et al 2016a), Kazakhstan (L. Agafonov, A. Berdnokova, unpubl. data), and Uzbekistan (Seim et al 2016b).

European Russia is also an area where ancient populations traditionally used wood for construction, heating, and other purposes. The original old-growth forests were also cleared for agriculture. These activities, along with climate contributing to the rapid decay of wood, are the reasons why old wood collections are quite rare in the region. After the archaeological Novgorod chronology (Kolchin 1963) was constructed, only a few composite chronologies based on archeological, architectural, and modern (living) wood samples covering a substantial part of the past millennium have been constructed (Solomina et al 2011; Karpukhin and Matskovsky 2014; Solomina et al 2017; Tarabardina 2009; Kulakova 2009). This limits the useful length to the ERDA to 1400-2016 CE at present.

4. Methods

A. Tree-ring standardization

The 697 tree-ring chronologies used for reconstruction were standardized (sensu Fritts 1976) in a relatively uniform way using state-of-the-art tree-ring standardization methods based on 'signal free' detrending (Melvin and Briffa 2008) to eliminate trend-distortion artefacts and maximally preserve common medium frequency variance among series. In addition, we used the age-dependent spline (Melvin and Briffa 2007) to conservatively remove low-frequency variance thought to be mainly due to non-climatic age/size-related changes in ring width over time. This combination minimizes the loss of common variance due to the 'segment length curse' (Cook et al 1995). In addition, adaptive power transformations were applied to the raw ring-width measurements prior to detrending to render them more homoscedastic. Doing so enabled the tree-ring indices to be calculated as residuals rather than ratios to reduce the likelihood of index calculation bias in the estimation of the tree-ring chronologies (Cook and Peters 1997).

B. Ensemble Point-by-Point Regression

Ensemble Point-by-Point Regression (EPPR) was used to produce the ERDA. It is a generalization of the original PPR method (Cook et al 1999) whereby each tree-ring chronology found within a given search radius around each grid point is weighted by some power of its correlation with the climate variable being reconstructed. See Cook et al (2013, 2015) and the Supplementary Materials for details. The correlation-weighted chronologies are then used in the principal components regression (PCR) model at each grid point for reconstructing climate from tree rings. This is done in lieu of selecting a subset of chronologies based on a fixed correlation screening probability. For the ERDA we used two tree-ring search radii, 500 and 1000 km, for locating the tree-ring chronologies for reconstructing each scPDSI grid point. This resulted in a 16-member ensemble (eight per search radius), which was then robustly averaged for further use.

The EPPR method used here is identical to that used in creating the OWDA (Cook et al 2015), which makes a one-to-one comparison of calibration and validation skill between the two drought atlases possible for the common region of overlap indicated in Fig. 1. This comparison will be shown later.

C. Queen's Case Imputation and Smoothing

Here we introduce Queen's Case Imputation and Smoothing (QCIS) and describe why it was developed. EPPR produces reconstruction fields that are spatially complete as far back as the first year of the shortest grid point reconstruction produced. Earlier than that, spatial gaps in the annual reconstructed fields develop, and these gaps increase in size back in time because some grid point reconstructions are longer than others due to the varying tree-ring chronology lengths used. In addition, there can be "checker board" patterns in the reconstructed fields produced in part by random effects in the EPPR procedure at the grid point level. These properties imply the need to both locally impute and smooth the ERDA fields in a way that is consistent with the pointwise regression design of EPPR.

To this end, we developed a 9-point regression kernel method called Queen's Case Imputation and Smoothing (QCIS) and applied it to each grid point reconstruction produced by EPPR to re-estimate, locally smooth, and infill spatial gaps in the fields back to 1400 CE. For consistency with the original EPPR results, QCIS uses the same PCR method as EPPR, the same grid point instrumental data for recalibration, and reports the same calibration/validation period statistics. Thus, QCIS is designed to produce a locally smoothed and infilled field reconstruction that is consistent with the original pointwise design of PPR (Cook et al 1999). See the Supplementary Materials for details.

D. Calibration and Validation

The instrumental scPDSI data used for statistical calibration and validation cover the 1901-2016 period. In contrast, the tree-ring chronologies have a common end year of 1983 because of the widely varying years in which the trees were sampled. For this reason, the calibration period chosen for developing the reconstructions was 1931-1983. The remaining 1901-1930 scPDSI data were withheld from the calibration exercise for use in model validation testing (Berk 1984; Picard and Berk 1990). This style of split calibration/validation testing is described in Fritts (1976) and has been used successfully in the development of all previous drought atlases beginning with Cook et al (1999).

The calibration period statistics reported here are the coefficient of determination (R^2 or CRSQ) and a leave-one-out cross-validation statistic (CVRE). CVRE is the R^2 version of the Prediction Error Sum of Squares (PRESS) statistic (Allen 1974; Quan 1988) and, thus, provides a less biased expression of explained variance compared to CRSQ. In poorly calibrated cases, CVRE can actually be negative, which is impossible for CRSQ.

The validation statistics reported here are the square of the Pearson correlation (VRSQ), the reduction of error (VRE), and the coefficient of efficiency (VCE). When VRSQ, VRE, and VCE are positive, they are different measures of model skill expressed in units of fractional explained variance over the validation period. Negative values indicate no reconstruction skill as measured. In addition, the formulae of these statistics require that VRSQ≥VRE≥VCE when calculated from the same data, thus making VCE the hardest validation statistic to pass. See Cook et al (1994, 1999) for detailed descriptions of these model validation statistics.

5. Calibration and Validation Results

The ERDA calibration and validation maps based on the EPPR 16-member ensemble mean field are shown in Fig. 2. Overall, the calibration period CRSQ exceeds 40% of the total scPDSI variance

at most grid points. The same is true for the leave-one-out CVRE. The weakest CRSQ and CVRE statistics are found in the southeast quadrant of the domain near the Caspian and Aral Seas where there are very few tree-ring chronologies (see Fig. 1). Weaker, but still useful, reconstruction skill over the validation period is indicated by positive VRSQ, VRE, and VCE over much of the domain, with the weakest results again in the southeast quadrant and also in the area above 60-65°N where tree-ring drought sensitivity is likely to be weaker (Matskovsky 2016). The lower right-hand map is the average correlation (RBAR) between the 16 EPPR ensemble members. The typical correlation falls in the 0.5-0.7 range, which illustrates how the differential correlation weighting and search radii used by EPPR produces a range of reconstruction outcomes.

The calibration and validation results presented in Figs. 2 strongly supports the overall validity of the ERDA. Nonetheless, it is useful to show the degree to which they are better than those of the OWDA in the overlapping domain regions shown in Fig. 1. Figure 3 compares the ERDA and OWDA using two calibration statistics (CRSQ and CVRE) and one validation statistic (VRSQ). This comparison shows that the ERDA is far more skillful than the OWDA over their shared domains. Since the scPDSI data and EPPR methods used are the same for each drought atlas, the only plausible explanation for the improved calibration/validation skill in the ERDA is its vastly improved tree-ring network used for reconstruction.

6. Rotated EOF Analysis

The ERDA is made up of 4,259 grid points of one-half degree scPDSI covering the common period 1400-2016. As described earlier, complete spatial coverage back to 1400 was achieved by applying QCIS to the original ensemble member fields before averaging. In the process, QCIS locally smoothed the fields to reduce “checker board” patterns. See the Supplementary Materials for details. QCIS was applied to all data up to 2016, but only the data up to 1983 are based on tree-ring estimates. It is the tree-ring-only portion of the ERDA from 1400 to 1983 that will be evaluated now using empirical orthogonal function (EOF) analysis.

EOF analysis has a long history of use in climatological studies (e.g. Lorenz 1956; Kutzbach 1967) and in tree-ring analyses (e.g. LaMarche Jr. and Fritts 1971; Fritts 1976) because it distills the complex variability contained in a sequence of climate and tree-ring fields into a greatly reduced subset of orthogonal fields for potentially easier interpretation and application. However, as pointed out by Richmond (1986), care must be applied in interpreting EOFs as realistic expressions of natural climate variability because of the mathematical constraints applied to their estimation. See also Hannachi et al (2007) and Monahan et al (2009) for more recent reviews that detail the limitations of EOFs for climatological interpretation.

A common way to reduce the well known limitations of EOFs for physical interpretation is to apply analytical rotation to a subset of EOFs. There are many ways to do this (Richman 1986), but we chose here the widely used normalized Varimax method (Kaiser 1958). This rotation method has been used with considerable success in characterizing the space-time patterns variability of climate fields, such as those related to the quasi-stationary modes of upper-air atmospheric circulation (Barnston and Livezey 1987) and to fields of PDSI based on both instrumental (Karl and Koscielny 1982) and reconstructed (Cook et al 1999) data.

The application of Varimax rotation requires a reasonably well estimated subset of EOFs (the "signal subspace") to rotate. There are many ways this might be determined (Preisendorfer et al 1981), but it is complicated by the rank deficiency of the ERDA correlation matrix, which is based on 4,259 (m) grid points and 584 (n) years of data. For centered data, the total number of defined EOFs is $min(n\text{-}1,m)$, or only 583 in the case of the ERDA. This renders asymptotic methods such as the Kaiser-Guttman eigenvalue-1 cutoff rule (Guttman 1954; Kaiser 1960) quite useless to apply. It also degrades the performance of monte-carlo methods like the 'Rule N' method (Preisendorfer et al 1981). Therefore, we have chosen a very simple method based on the visual scree test of the eigenvalue trace (Cattell 1966), with the added application of the "North test" for separation of eigenvalues (North et al 1982).

Figure 4 shows the eigenvalue trace out to order-10 calculated from the ERDA correlation matrix. There is no point in showing more because the cumulative variance trace shows that the first ten eigenvalues already accounts for 73.9% of the total variance. Each eigenvalue has its uncertainty expressed as ±2 standard errors as estimated by the equation provided by North et al (1982). The first three eigenvalues separate cleanly from the rest, even after considering their 2-standard error uncertainties, and account for 42.5% of total variance. This indicates that there are only three EOFs in the signal subspace worth rotating. The sharp break in the eigenvalue trace after the third eigenvalue may reflect in part the application of QCIS to the ERDA because QCIS will emphasize larger-scale patterns due to its spatial smoothing effect.

The EOFs before and after rotation (the Varimax factors or VFs) are shown in Fig. 5 for comparison, along with the variance accounted for by each. There is relatively little difference between them, and the total variance (42.5%) after rotation is exactly conserved as required by the Varimax method. However, the regional expressions of drought and wetness are more cleanly separated after rotation. They represent three principal areas of the ERDA domain: interior European Russia east of ~40°E (VF1), cool northwestern Russia and the Baltic region (VF2), and western Russia, Belarus, and Ukraine (VF3). The area most weakly represented by any of these factors is in the southeastern quadrant where calibration was relatively weak (Fig. 2) and the effect of QCIS was the greatest (Fig. SM4).

Figure 6 shows plots of the VF scores (Figs. 6a-c) corresponding to their respective factor patterns shown in Fig. 5. In addition, the mean of the three factor scores (Fig. 6d) is intended to highlight occurrences of 'pan-ERDA' dry and wet years. Since the Varimax factor scores are orthogonal, the mean should preserve the occasional years when these events co-occur and at the same time dampen out other variability not common to the three factors.

Each series has been expressed in terms of standard deviations from the mean, with a 10-yr low-pass filter (red) applied to each to emphasize mult-year variability in drought and wetness. The horizontal dashed lines are the ±2 standard deviation limits used for identifying years of severe

drought and wetness. Notable years of severe drought are 1936, 1841, 1757 for VF1, 1408, 1940, 1826 for VF2, and 1453, 1921, 1939 for VF3. The top three drought years in the mean 'pan-ERDA' series are 1939, 1921, and 1659. A complete list of dry and wet years exceeding ±2 standard deviation limits in Fig. 6 is provided in Table 1. Overall, there is a somewhat higher frequency of extreme drought years indicated since 1800, with 1921 and the 1930s standing out in particular. In contrast, unusually wet years appear to be more evenly distributed over time.

Using the factor scores plotted in Fig. 6a-c, additional validation testing was conducted on the ERDA. This was done using GPCC precipitation, BEST temperature, and UCAR scPDSI gridded data (refer to "Climate data sets" above) for the same JJA season as the ERDA reconstruction. The 1891-1930 pre-calibration period was used for these "out-of-sample" tests of the ERDA factor scores based now on ten additional years of data over that used previously for validation.

Figure 7 shows correlation maps for Varimax factors VF1-VF3 versus GPCC, BEST, and UCAR climate data. Correlations >|0.4| are significant at the 99% confidence level. The rectangle shown in each map delineates the boundaries of the ERDA. After comparing the GPCC, BEST, and UCAR correlation patterns with the Varimax factor patterns (Fig. 5), the highest climate correlations can be seen to largely fall in the same locations as the highest factor loadings, a result that supports the climate interpretations of these modes. In particular, the temperature correlation pattern in VF1 is similar to the East Atlantic/Western Russia (EA/WR) pattern for summer (Barnston and Livezey 1987; their Eurasia-2 pattern), with the main center of action north of the Black and Caspian Seas. The strongest monthly correlation between the EA/WR index and VF1 is for May ($r=0.45$, $p<0.01$) for the 1950-1983 period. There is also some similarity between VF2 and the Scandinavian (SCAND) pattern (Barnston and Livezey 1987; their Eurasia-1 pattern), characterized by a meridional dipole in both temperature and precipitation with a strong locus over Scandinavia. In this case the strongest correlation between SCAND and VF2 is for the month of March ($r=-0.48$, $p<0.01$).

Schubert et al (2014) applied rotated EOF (REOF) analysis to the joint summer (JJA) temperature and precipitation fields over northern Eurasia, which fully includes the ERDA domain. Their REOF1 temperature and precipitation factor patterns (Fig. 3 in Schubert et al 2014) include high loadings over the ERDA VF1 region. Similar spatial congruence can also be found between their REOF5 factor patterns and that shown here in VF3. Given the relatively short analysis period (1979-2012) used by Schubert et al (2014), plus their much larger analysis domain, this level of agreement suggests a robust link between the hydroclimatic variability expressed in the ERDA and much larger scale atmospheric circulation features across all of northern Eurasia.

Figure 8 shows composites of the notable dry and wet years indicated in Fig. 6 and listed in Table 1. For the most part the dry and wet composites are near-mirror images of each other, suggesting a linear association between the occurrence of these extreme patterns and their causal mechanisms. The clear exception is the asymmetry in the patterns associated with VF3 over western Russia, Belarus, and Ukraine. The dry year pattern extends zonally across most of European Russia, with a small pattern of wetness north of about 62°N. In contrast, the VF3 wet year pattern exhibits a strongly meridional west-to-east change from wet to dry.

The ERDA factor scores do not reveal the occurrence of severe long-duration droughts (i.e. megadroughts) over European Russia and surrounding countries like those found in the American West (Cook et al 2004). This is consistent with the understanding that individual drought events across European Russia rarely exceed 50 days in duration (Cherenkova 2007; Schubert et al 2014). The longest period of mostly below-average scPDSI in the ERDA factor scores occurred over a 26-year period from 1784 to 1809. Few individual drought years stand out during this time, but the overall cumulative moisture deficit would have been large. This period of persistent drought is most prominent over interior European Russia east of 40°E (VF1) and western Russia, Belarus, and Ukraine (VF3). In support of this result, Borisenkov and Pasetsky (1988, 2003) list several years of drought that occurred in European Russian during this time. Interestingly, this was also a time of a “major long-duration drought” over England and Wales from 1798 to 1808 (Cole and Marsh 2006), and also over north-central Europe as reconstructed by the OWDA (Cook et al

2015). Connection of hydroclimate in the center of European Russia and Eastern Europe was also noted by Matskovsky et al (2017).

7. Comparison to historical droughts

Table 1 highlights in bold red the years for which there are some historical references of droughts at various locations in European Russia (e.g. Borisenkov and Pasetsky 1988, 2003; Kahan 1968). Fewer, but still noteworthy, years of unusual wet conditions are highlighted in bold blue. In each case, the source references for those years are noted. There may be a historical bias in recording the negative impacts of droughts more frequently than the positive impacts of wet events, but this is impossible to know for sure. Also, the quality of the historical data very likely degrades back time from loss of records and changes in reporting locations, thus making definitive comparisons between the ERDA and historical references difficult to judge. Nevertheless, both the VF1 and mean VF1-3 dry extremes have historical references for 12 out of 16 and 11 out 16 dry years, respectively. Thus, there are many more historical dry "hits" than "misses" overall in the ERDA. The cause for some of these dry "misses" is hard to ascertain. Some may simply be due to inadequate historical data. They could also be associated with unusually cold winter/spring conditions over European Russia (Borisenkov and Pasetsky 1988, 2003; see Table SM1 for examples), which may have suppressed radial tree growth and thus mimicked the narrow rings more frequently associated with drier conditions. Those suggested years are highlighted in parentheses in the "WET" list in Table 1.

Table B1 in Schubert et al (2014) also provides a list of droughts and heat waves affecting Eurasia since 1875 based on historical information. We created a composite map from the ERDA of the ten major drought years from that list up to 1930 in Table B1 to avoid biasing the outcome with data from the calibration period. The ten-year composite (lefthand map) and where its regional mean is statistically significant (righthand map) are shown in Fig. 9, with the specific years used listed in the figure caption. The composite is statistically signficant over European Russia south

497 of ~56°N, an area that is important to Russian grain production. It is also the area covered mostly
498 by VF3.
499
500 ## 8. Links to Atmospheric Circulation
501
502 To better understand the likely atmospheric dynamics behind the hydroclimatic patterns
503 expressed by the ERDA Varimax factors, the correlations between their factor scores (Fig. 6) and
504 700 hPa heights and 200 hPa meridional winds from the 20th Century Reanalysis (Compo et al
505 2011) are shown in Fig. 10. All calculations were done on the tree-ring only estimates over the
506 1880-1983 period. The season with the best correlations is May-June-July, beginning one month
507 earlier than the June-July-August scPDSI season. This earlier atmospheric dynamics association
508 with summer drought is similar to that found by Rocheva (2012) in her study of "possible
509 forerunners of droughts", which are linked to the development of persistent anticyclones, drying,
510 and heat waves over Russia (Schubert et al 2014).
511
512 Overall, the locations of the significant negative correlations (blue) with the pressure field are
513 precisely where they should be expected given the locations of the strongly positive (red) factor
514 loadings. Secondary positive correlations (orange) with the pressure field are located southward
515 over the Levant (VF1), southern Volga/Urals (VF2), and northwest Africa (VF3) regions. The
516 circulation pattern associated with VF1, in particular, shows a strong similarity to the circulation
517 anomalies during the mid-summer of 2010. Characterized by anticyclonic circulation over
518 European Russia and low pressure east of the Caspian sea, this is the pattern that drove the
519 concurrent extremes (drought over Russia; floods over Pakistan) that year (Lau and Kim, 2011).
520 Additionally, correlations with the 200 hPa meridional winds are quite similar to the correlation
521 patterns between the joint temperature and precipitation rotated principal components (RPCs)
522 and 250 hPa meridional winds in Schubert et al (2014) (Fig. 6, therein). Correlations with VF1, for
523 example, show strong similarity to the correlation pattern with RPC1 in Schubert et al (2014),
524 characterized by anti-phased correlations over Scandinavia and Russia northeast of the Caspian
525 Sea. VF2 from the ERDA is also similar to RPC5 in Schubert et al (2014), with major centers of

action centered north of Great Britain and over Finland. Along with the previous temperature and precipitation comparisons, these results suggest that the ERDA accurately captures the dominant modes of spatiotemporal climate variability within the region.

9. Conclusions

The European Russia Drought Atlas (ERDA) is an important new paleoclimatic reconstruction that greatly advances our understanding of spatio-temporal hydroclimatic variability over the East European Plain. It is a one-half degree gridded reconstruction of summer scPDSI, covering the period 1400-2016 CE, which was made possible by the development of a critically important new tree-ring network for European Russia and surrounding countries. An ensemble version of the point-by-point regression method (EPPR) was used to reconstruct scPDSI at the grid point level, which makes it compatible with other paleo-drought atlases based on tree rings, including the proximal Euro-Mediterranean OWDA.

The ERDA has demonstrated skill when compared to instrumental data at the grid point level and compares favorably to recorded instances of historical droughts over European Russia extending back to the 15th Century. It is also spatially complete back to 1400 due to the application of a local imputation and smoothing method specifically designed to be compatible with the EPPR reconstruction method. Rotated EOF analysis reveals three principal modes of varability in the ERDA that have links to large-scale atmospheric circulation dynamics over northern Eurasia associated with the development of droughts and heat waves there. The planned geographic expansion of this drought atlas to cover all of northern Eurasia is therefore expected to yield a much more complete understanding of hydroclimatic variability and its causes.

Acknowledgements

Funding for this study was provided to E.R.C. by the Center for Climate and Life at the Lamont-Doherty Earth Observatory of Columbia University. The development of the new tree-ring

network in European Russia was spearheaded by O.S. and V.M. through their many contacts with tree-ring scientists in Russia and surrounding countries who generously contributed their tree-ring data for use. The list of co-authors reflects these many contributions. O.S. and V.M. have also received support from the State assignment project no. 0148- 2019-0004 (AAAA-A19-119022190172-5). L.A. received financial support from the State Contract of the Institute of Plant and Animal Ecology, UB RAS (project no. AAAA-A19-119031890086-0) and Russian Fund for Basic Researches (project no. 19-05-00591). E.D. was supported by the Russian Science Foundation project no. 17-77-20123. D.T. was supported by the Russian Foundation for Basic Research and by the Government of the Republic of Tatarstan within the framework of the research project no. 18-44-160028. M.Y. is grateful to the staff of Laboratory of Productivity & Stability of Plant Communities, Institute of Experimental Botany National Academy of Science of Belarus for their help in collection of samples. The ERDA is archived for public availability with the National Centers for Environmental Information, NESDIS, NOAA, U.S. Department of Commerce (). Lamont-Doherty Earth Observatory Contribution No. XXXX.

References

Agafonov LI, Gurskaya MA (2012) Effect of the longitudinal temperature gradient on the Main Radial Growth of Forest Trees North-West Siberia. Izvestiya Rossiiskoi Akademii Nauk. Seriya Geograficheskaya 5:48-60. (in Russian)

Agafonov LI, Gurskaya MA (2013) The Influence of the Lower Ob River Runoff on Radial Growth of Trees. Contemp Probl Ecol 6:779–787.

Agafonov LI, Meko D, Panyushkina I (2016) Reconstruction of Ob River, Russia, discharge from ring widths of floodplain trees. J Hydrol 543:198-207.

Alisov BP (1969) Climate of the USSR. Izdatelstvo MGU, Moscow.

Allen DM (1974) The relationship between variable selection and data augmentation and a method for prediction. Technometrics 16:125–127.

Askeyev OV, Tishin DV, Sparks TH, Askeyev IV (2005) The effect of climate on the phenology, acorn crop and radial increment of pedunculate oak (Quercus robur) in the Middle Volga region, Tatarstan, Russia. Int J Biometeorology 49: 262-266.

Barnston AG, Livezey RE (1987) Classification, seasonality, and persistence of low-frequency atmospheric circulation patterns. Mon Weather Rev 115:1083–1126.

Berk KN (1984) Validating regression procedures with new data. Technometrics 26(4):331-338.

Bogolepov MA (1907) About climatic fluctuations of European Russia during historical time. Earth Sci (Zemlevedeniye) 3:1-188. (in Russian)

Bogolepov VA (1922) Causes of poor harvest and starvation in Russia in the historical period. Novaya Derevnya, Moscow. (in Russian)

Borisenkov EP, Pasetsky VM (1988) Thousand-Year Chronicle of Unusual Phenomena of Nature Mysl', Moscow. (in Russian)

Borisenkov EP, Pasetsky VM (2003) Chronicle of unusual natural event during the last 2.5 millennia. Gidrometizdat, St. Petersburg. (in Russian)

Buchinsky IE (1957) On the past climate of the Russian Plain. Gidrometizdat, Leningrad. (in Russian)

Buchinsky IE (1976) Droughts and Dry Winds. Gidrometeoizdat, Leningrad. (in Russian)

598 Cattell RB (1966) The scree test for the number of factors. Multivar Behav Res 1(2):245-276.
599 Cherenkova EA (2007) Dynamics of severe atmospheric droughts in European Russia. Russ
600 Meteorol Hydrol 32(11):675–682.
601 Chernavskaya M (1995) Intrasecular air temperature changes in the North European Russia over
602 the last millennium. International Conference on Past, Present and Future Climate. 22–25
603 August. Helsinki, Finland. P. 119–121.
604 Cole GA, Marsh TJ (2006) The impact of climate change on severe droughts. Major
605 droughts in England and Wales from 1800 and evidence of impact, in Science
606 Report:SC040068/SR1 (Environment Agency, Bristol, UK, 2006).
607 Compo GP, Whitaker JS, Sardeshmukh PD, Matsui N, Allan RJ, Yin X, Gleason BE, Vose RS,
608 Rutledge G, Bessemoulin P, Brönnimann S, Brunet M, Crouthamel RI, Grant AN, Groisman
609 PY, Jones PD, Kruk M, Kruger AC, Marshall GJ, Maugeri M, Mok HY, Nordli Ø, Ross TF,
610 TrigoRM, Wang XL, Woodruff SD, Worley SJ (2011) The Twentieth Century Reanalysis
611 Project. Q J Roy Meteor Soc 137:1-28.
612 Cook ER, Meko DM, Stahle DW, Cleaveland MK (1999) Droughtreconstructionsfor the
613 continental United States. J Clim 12:1145-1162.
614 Cook ER, Briffa KR, Jones PD (1994) Spatial regression methods indendroclimatology: a review
615 and comparison of two techniques. Int J Climatol 14:379-402.
616 Cook ER, Briffa KR, Meko DM, Graybill DA, Funkhouser G (1995) The segment length curse in
617 long tree-ring chronology development for paleoclimatic studies. Holocene 5(2):229-237.
618 Cook ER, Peters K (1997) Calculating unbiased tree-ring indices for the study of climatic and
619 environmental change. Holocene 7(3):359-368.
620 Cook ER, Woodhouse C, Eakin CM, Meko DM, Stahle DW (2004) Long-term aridity changes in
621 the western United States. Science 306:1015-1018.
622 Cook ER, Anchukaitis KJ, Buckley BM, D'Arrigo R, Jacoby GC, Wright WE (2010) Asian monsoon
623 failure and megadrought during the last millennium. Science 328:486-489.
624 Cook ER, Krusic PJ, Anchukaitis KJ, Buckley BM, Nakatsuka T, Sano M, Asia2k members (2013)
625 Tree-ring reconstructed summer temperature anomalies for temperate East Asia since
626 800 C.E. Clim Dyn 41:2957-2972. https://doi: 10.1007/s00382-012-1611-x.

627 Cook ER, Seager R, Kushnir J, Briffa KR, Buentgen U, Frank D, Krusic PJ, Tegel W, van der Schrier
628 G, Andreu-Hayles L, Baillie M, Baitttinger C, Bleicher N, Bonde N, Brown D, Carrer M,
629 Cooper R, Cufar K, Dittmar C, Esper J, Griggs C, Gunnarson B, Gunther B, Gutierrez E,
630 Haneca K, Helema S, Herzig F, Heussner K-U, Hofmann J, Janda J, Kontic R, Kose N, Kyncl T,
631 Levanic T, Linderholm H, Manning S, Melvin T, Miles D, Neuwirth B, Nicolussi K, Nola P,
632 Panayotov M, Popa I, Rothe A, Seftigen K, Seim A, Svarva H, Svoboda M, Thun T, Timonen
633 M, Touchan R, Trotsiuk V, Trouet V, Walder F, Wazny T, Wilson R, Zang C(2015) Old world
634 megadroughts and pluvials during the Common Era. Science Advances, vol. 1, no. 10,
635 e1500561, DOI: 10.1126/sciadv.1500561.
636 Dai A, Zhao T (2017) Uncertainties in historical changes and future projections of drought. Part
637 I: Estimates of historical drought changes. Climatic Change 144(3):519-533.DOI:
638 10.1007/s10584-016-1705-2.
639 Dolgova EA (2016) June–September temperature reconstruction in the Northern Caucasus
640 based on blue intensity data. Dendrochronologia 39:17-23.
641 Dronin NM, Bellinger EG (2005) Climate Dependence and Food Problems in Russia, 1900-1990:
642 The Interaction of Climate and Agricultural Policy and Their Effect on Food Problems.
643 Budapest, New York: Central European University Press, 2005.
644 Drozdov OA (1980) Droughts and Humidity Dynamics. Gidrometeoizdat, Leningrad. (In Russian)
645 Esper J, Shiyatov S, Mazepa V, Wilson R, Graybill D, Funkhouser G (2003) Temperature-sensitive
646 Tien Shan tree ring chronologies show multi-centennial growth trends. Clim Dyn 21:699–
647 706.
648 Fritts HC (1976) Tree Rings and Climate. Academic Press, New York.
649 Gazina EA, Klimenko VV (2008) Climatic changes of the Eastern Europe during the last 250 years
650 by instrumental data. Moscow University Bulletin. Series 5. Geography 3:60-66.
651 Gershunov A, Douville H (2008) Extensive summer hot andcold extremes under current and
652 possible future climaticconditions: Europe and North America. Climate Extremes and
653 Society, H. F. Diaz and R. J. Murnane, Eds., Cambridge University Press, pp. 74–98.

654 Golubev G, Dronin N (2004) Geography of Droughts and Food Problems in Russia (1900-2000),
655 Report No. A 0401. (Center for Environmental Systems Research, University of Kassel, Kurt-
656 Wolters-Str. 3, 34109 Kassel, Germany. (http://www.usf.uni-kassel.de)
657 Graybill D, Shiyatov S, Burmistrov V (1992) Recent dendrochronological investigations in
658 Kirghizia, USSR. Lundqua Rep 34:123-127.
659 Gurskaya M, Hallinger M, Singh J, Agafonov L, Wilmking M (2012) Temperature reconstruction
660 in the Ob River valley based on ring widths of three coniferous tree species.
661 Dendrochronologia 30(4):302-309.
662 Guttman L (1954) Some necessary conditions for common-factor analysis. Psychometrika
663 19:149–161.
664 Kahan A (1968) Natural calamities and their effect upon the food supply of Russia.
665 Jahrbücherfür Geschichte Osteuropas (Yearbooks for the history of Eastern Europe)
666 16(3):353-377.
667 Kaiser HF (1958) The Varimax criterion for analytic rotation in factor analysis. Psychometrika
668 23:187-200.
669 Kaiser HF (1960) The application of electronic computers to factor analysis. Educ Psychol Meas
670 20:141-151.
671 Karl TR, Koscielny AJ (1982) Drought in the United States. J Clim 2:313–329.
672 Karpukhin AA, Matskovsky VV (2014) Absolute generalized tree-ring chronology of Sheksna and
673 Sukhona rivers catchments (AD 1085-2009). Russ Archaeol 2:76-87. (in Russian)
674 Kiselev S, Romashkin R, Nelson GC, Mason-D'Croz D, Palazzo A (2013) Russia's food security and
675 climate change: Looking into the future. Economics: The Open-Access, Open-Assessment
676 E-Journal 7:2013-2039.
677 Kleschenko AD (2005) Monitoring agricultural drought in Russia. In: Boken, V, Cracknell, AP,
678 Heathcote, RL, Eds., Monitoring and Predicting Agricultural Drought, Oxford University
679 Press, 196–207.
680 Klimanov VA, Khotinsky NA, Blagoveshenskaya NV (1995) Climate fluctuations during the
681 historical times in the center of Russian Plain. Izvestiya Rossiiskoi Akademii Nauk. Seriya
682 Geograficheskaya 1:89–96. (in Russian)

683 Klimenko V, Solomina ON (2010) Climatic variations in the East European Plain during the last
684 millennium: state of the art. In R. Przybylak et al (eds.), The Polish Climate in the European
685 Context: An Historical Overview, DOI 10.1007/978-90-481-3167-9_3. Springer
686 Science+Business Media B.V., pp. 71-102.
687 Knysh NV, Yermokhin MV (2019) The effects of climatic factors in forming increment of English
688 oak (Quercus robur L.) in south regions of Belarus. Proceedings of the National Academy of
689 Science of Belarus. Biological Series 64(2):169-179. (in Russian)
690 Kolchin BA (1963) Dendrochronology of Novgorod. In: Materials and Research of Archaeology of
691 USSR. AN SSSR, Moscow. (in Russian)
692 Krenke AN, Chernavskaya MM (1998) Spatial and temporal variations of the frequency of
693 extreme climatic events in the Russian Plain. Izvestiya Rossiiskoi Akademii Nauk. Seriya
694 Geograficheskaya 5:53-61.
695 Kulakova M (2009) A dendrochronological analysis of wood from Pskov. Archaeol Ethnol
696 Anthropol Eurasia 37(1):71-76.
697 Kupfer AYa (1846) Conclusions from meteorological records performed in the Russian State and
698 stored in the meteorological archive of Academy of Sciences. Academy of Sciences, St.
699 Petersburg.
700 Kutzbach JE (1967) Empirical eigenvectors of sea-level pressure, surface temperature and
701 precipitation complexes over North America. J Appl Meteorol 6:791–802.
702 LaMarche Jr VC, Fritts HC (1971) Anomaly patterns of climate over the western United
703 States,1700-1930, derived from principal component analysis of tree-ring data. Mon
704 Weather Rev 99:139-142.
705 Lau WK, Kim KM (2012). The 2010 Pakistan flood and Russian heat wave: Teleconnection of
706 hydrometeorological extremes. J Hydrometeor 13(1):392-403.
707 Lorenz EN (1956) Empirical orthogonal functions and statistical weather prediction. Statistical
708 Forecasting Project Report 1, MIT Department of Meteorology, 49 pp.
709 Matskovsky V (2016) Climatic signal in tree-ring width chronologies of conifers in European
710 Russia. Int J Climatol 36:3398-3406.

711 Matskovsky V, Dolgova E, Lomakin N, Matveev S (2017) Dendroclimatology and historical
712 climatology of Voronezh region, European Russia, since 1790s. Int J Climatol 37:3057-3066.
713 Matveev SM, Tarankov VI, Shurygin YN (2012a) Dendroclimatological analysis of the natural
714 forest and forest plantations of scots pine (Pinussylvestris L.) in dry-moist site conditions of
715 the Khrenovoe pine forest. Nauchn zh Kuban gosagraruniv 75(1):1–12. (in Russian)
716 Matveev SM, Matveeva SV, Shurygin YN (2012b) Recurrence of severe droughts and long-term
717 dynamics of radial increment of the scots pine in the Usman and Khrenovoe forests in the
718 Voronezh region. J Sib Federal Univ Biol 5(1):27–42. (in Russian)
719 Melvin TM, Briffa KR, Nicolussi K, Grabner M (2007) Time-varying-response smoothing.
720 Dendrochronologia 25:65–69.
721 Melvin TM, Briffa KR (2008) A “Signal-Free” approach to dendroclimaticstandardisation.
722 Dendrochronologia 26:71–86.
723 Meshcherskaya AV, Blazhevich VG (1997) The drought and excessive moisture indices in a
724 historical perspective in the principal grain-producing regions of the former Soviet Union. J
725 Clim 10:2670-2682.
726 Muller RA, Curry J, Groom D, Jacobsen R, Perlmutter S, Rohde R, Rosenfeld A, Wickham
727 C,Wurtele J (2013) Decadal variations in the global atmospheric land temperatures. J
728 Geophys Res-Atmos 118, doi:10.1002/jgrd.50458.
729 Neumann J, Lindgrén S (1979) Great historical events that were significantly affected by the
730 weather: 4, The great famines in Finland and Estonia, 1695–97. Bull Amer Meteor
731 Soc 60(7):775–787.
732 North GR, Bell TL, Cahalan RF, Moeng FJ (1982) Sampling errors in the estimation of empirical
733 orthogonal functions. Mon Weather Rev 110:699–706.
734 Obukhov AM, Kurganskii MV, Tatarskaya MS(1984) Dynamical conditions of drought and other
735 large-scale weatheranomalies formation. Sov. Meteor. Hydrol. 10:5–13. (in Russian)
736 Osborn TJ, Barichivich J, Harris I, van der Schrier G, Jones PD (2017) Monitoring global drought
737 using the self-calibrating Palmer Drought Severity Index [in "State of the Climate in
738 2016"]. B Am Meteorol Soc 98:S32-S33.

739 Pavlova V, Shkolnik I, Pikaleva A, Efimov S, Karachenkova A, Kattsov V (2019) Future changes in
740 spring wheat yield in the European Russia as inferred from a large ensemble of high-
741 resolution climate projections. Environ Res Lett 14:034010.
742 Picard RR, Berk KN (1990) Data splitting. Am Stat 44:140-147.
743 Preisendorfer RW, Zwiers FW, Barnett TP (1981) *Foundations of Principal Component Selection*
744 *Rules*. SIO Reference Series 81-4, Scripps Institution of Oceanography, 192 pp.
745 Pushin AV, Chernavskaya MM, Chernikh NB (2004) Climatic extremes and growth anomalies of
746 wood in 16-19 centuries in the north of the Russian. Russian Archaeology 4:86-99.
747 Quan NT (1988) The prediction sum of squares as a general measure for regression diagnostics.
748 *J Bus & Econ Stat* 6:501-504.
749 Rauner YuL(1981) Dynamics of humidity extremes in historical period. Izvestiya Rossiiskoi
750 Akademii Nauk. Seriya Geograficheskaya 6:5-22. (in Russian)
751 Richman MB (1986) Rotation of principal components. J Clim 6:293–335.
752 Rocheva EV (2012) Possible forerunners of droughts in agricultural areas of Russia. Russ
753 Meteorol Hydrology 37:575–585.
754 Rudenko AI, Ed. (1958) Droughts in the USSR. Their Origin, Frequency of Occurrence and
755 Impact on Yield. Gidrometeoizdat, Leningrad. (in Russian)
756 Schneider U, Becker A, Finger P, Meyer-Christoffer A, Ziese M (2018) GPCC Full Data Monthly
757 Product Version 2018 at 1.0°: Monthly Land-Surface Precipitation from Rain-Gauges built
758 on GTS-based and Historical Data. DOI: 10.5676/DWD_GPCC/FD_M_V2018_100.
759 Shostakovich VB (1934) Silt lake deposits and periodic variations of natural events. Zapiski
760 Gosudarstvyenogo Gidrologicheskogo Instituta 13:94–108.
761 Schubert SD, Wang H, Suarez M (2011) Warm season subseasonal variability and climate
762 extremes in the Northern Hemisphere: The role of stationary Rossby waves. J Clim
763 24:4773–4792, doi:10.1175/JCLI-D-10-05035.1.
764 Schubert SD, Want H, Koster RD, Suarez MJ, Groisman PY(2014) Northern Eurasian heat waves
765 and droughts. J Clim 27:3169-3207.
766

767 Schubert SD, Stewart RE, Wang H, Barlow M, Berbery EH, Cai W, Hoerling M, Kanikicharla K,
768 Koster R, Lyon B, Mariotti A, Mechosa CR, Müller O, Rodriguez-Fonseca B, Seager R,
769 Seneviratne SI, Zhang L, Zhou T (2016). Global meteorological drought: a synthesis of
770 current understanding with a focus on SST drivers of precipitation deficits. J Clim
771 29(11):3989-4019.
772 Seim A, Omurova G, Azisov E, Musuraliev K, Aliev K, Tulyaganov T, Nikolyai L, Botman E, Helle G,
773 Liñan ID, Jivcov S, Linderholm HW (2016a) Climate change increases drought stress of
774 juniper trees in the mountains of Central Asia. PLoS ONE 11(4): e0153888.
775 doi:10.1371/journal.pone.0153888.
776 Seim A, Tulyaganov T, Omurova G, Nikolyai L, Botman E, Linderholm HW (2016b)
777 Dendroclimatological potential of three juniper species from the Turkestan range,
778 northwestern Pamir-Alay Mountains, Uzbekistan. Trees 30:733-748.
779 Shvedov FN (1892) Tree as a chronicle of droughts. Meteorol Bull 5:37-49.
780 Solomina O, Davi N, D'Arrigo R, Jacoby G (2005) Tree-ring reconstruction of Crimean drought
781 and lake chronology correction. Geophys Res Lett, 32, L19704.
782 doi:10.1029/2005GL023335.
783 Solomina ON, Matskovsky VV, Zhukov RS (2011)The Vologda and Solovki dendrochronological
784 “chronicles” as a source of information about the climate conditions of the last
785 millennium. Dokl Earth Sci 439:1104–1109. doi 10.1134/S1028334X11080071.
786 Solomina ON, Dolgova EA, Maximova OE (2012) Tree-Ring Based Hydrometeorological
787 Reconstructions in Crimea, Caucasus and Tien-Shan. Nestor Istoriya, Moscow, St.
788 Petersburg.
789 Solomina O, Maximova O, Cook E (2014) Picea schrenkiana ring width and density at the upper
790 and lower tree limits in the Tien Shan mts Kyrgyz republic as a source of paleoclimatic
791 information. Geography, Environment, Sustainability 1(7):66–79.
792 Solomina ON et al (2017) Droughts of the East European Plain according to
793 hydrometeorological and tree-ring data. Nestor Istoriya, Moscow, St. Petersburg.
794 Stefanon M, D’Andrea F, Drobinski P (2012) Heatwaveclassification over Europe and the
795 Mediterranean region. Environ Res Lett 7, 014023, doi:10.1088/1748-9326/7/1/014023.

796 Tarabardina OA (2009) Environmentand human behavior in northern dendrochronological
797 studies of medieval Novgorod Novgorod (Based on the findings of archaeological
798 excavations 1991–2006). Archaeology, Ethnology, Anthropology of Eurasia 37(1):77-84.
799 Tishin DV, Chizhikova NA, Chugunov RG (2014) Radial growth of pine (Pinus sylvestris L.)
800 swamps as an indicator of local climate change. Forestry bulletin 5: 177-182. (in Russian)
801 van der Schrier G, Barichivich J, Briffa KR, Jones PD (2013) A scPDSI-based global data set of dry
802 and wet spells for 1901-2009. J Geophys Res-Atmos 118:4025-4048.
803 van Oldenborgh GJ, Burgers G (2005) Searching for decadal variations in ENSO precipitation
804 teleconnections. Geophys Res Lett, 32, 15, L15701, doi:10.1029/2005GL023110.
805 Veselovsky KS (1857) On the climate of Russia. Imperial Academy Press, St. Petersburg. (in
806 Russian)
807 Voronov AM (1992) Estimate of the regional changes of hydroclimatic conditions at the
808 European part of Soviet Union according to historical data. Water Res 4:97–105. (in
809 Russian)
810 Vil'd GI (1882) New normal and five years mean air temperature. Imperial Academy Press, St.
811 Petersburg. (in Russian)
812 Wahlén E (1886) True daily means and daily variation of temperature at 18 stations of the
813 Russian Empire. Meteorologic Sbornik 3, 586 pp.
814 Wells N, Goddard S, Hayes MJ (2004) A self-calibrating Palmer Drought Severity Index. J Clim
815 17:2335–2351.
816 Yermokhin MV, Knysh NV (2016) Climate and grazing impact on a radial increment of oak
817 (Quercus robur L.). Natural Resources 2:67-74. (in Russian)
818 Zveryaev II, Allan RP (2010) Summertime precipitation variability over Europe and its links to
819 atmospheric dynamics and evaporation, J Geophys Res 115, D12102,
820 doi:10.1029/2008JD011213.
821
822
823
824

825 **Table:**

826

Table 1. Lists of driest and wettest years in the three Varimax factors estimated from the ERDA (1400-1983), plus the mean of those scores, all scaled in units of standard deviation from the mean. The driest and wettest years are selected as those that equal or exceed ±2 standard deviations from the mean. Three years with units exceeding ±1.99 standard deviations are also considered close enough to include in these lists. The years in bold red and blue are those years for which there are historical references to dry and wet conditions at various locations in European Russia. These locations are often non-specific, however. Years in parentheses are those that were reconstructed wet, but were historically noted to be dry.

VF1 DRY		VF2 DRY		VF3 DRY		MEAN VF1-3 DRY	
YEAR	<-2SD	YEAR	<-2SD	YEAR	<-2SD	YEAR	<-2SD
1936[2,3]	-3.897	**1408**[1,2]	-3.547	1453	-3.560	**1939**[2,3]	-3.336
1841[1]	-3.106	1940	-2.952	**1921**[3]	-2.717	**1921**[3]	-3.316
1757[1]	-2.904	**1826**[1]	-2.721	**1939**[2,3]	-2.682	1659	-3.109
1802[1]	-2.888	1941	-2.361	1659	-2.624	**1936**[2,3]	-2.949
1921[3]	-2.661	**1889**[1,2,3]	-2.356	**1660**[1]	-2.524	**1533**[1,2]	-2.777
1759[1]	-2.474	**1533**[1,2]	-2.258	1797	-2.481	**1757**[1]	-2.520
1433	-2.355	**1876**[1]	-2.206	**1891**[1,2,3]	-2.394	**1759**[1]	-2.472
1686	-2.219	1689	-2.201	1952	-2.293	**1827**[1]	-2.430
1795[1]	-2.206	1736	-2.117	**1747**[1,2]	-2.206	**1658**[1]	-2.329
1803[1]	-2.175	**1914**[1,2,3]	-2.078	1661	-2.183	1531	-2.266
1533[1,2]	-2.163	**1847**[1]	-2.042	**1848**[1,2]	-2.151	1940	-2.258
1434	-2.061	**1875**[1,2,3]	-2.031	1964	-2.110	**1826**[1]	-2.219
1911[2,3]	-2.040	1942	-2.003	**1748**[1,2]	-2.034	1532	-2.213
1417	-2.000	1845	-2.003			**1848**[1,2]	-2.039
1431[1,2]	-1.999	1532	-2.003			1787	-2.002
1934[2,3]	-1.991					**1897**[1,2,3]	-1.999
VF1 WET		**VF2 WET**		**VF3 WET**		**MEAN VF1-3 WET**	
YEAR	**>2SD**	**YEAR**	**>2SD**	**YEAR**	**>2SD**	**YEAR**	**>2SD**
1466	4.201	1453	2.684	**(1772)**[1]	2.731	**1509**[1]	2.683
1699[1]	2.877	**1695**[1,4]	2.543	1980	2.704	**(1772)**[1]	2.602
(1643)[1]	2.444	1962	2.469	1433	2.627	1482	2.491
1465	2.419	**(1892)**[1,2,3]	2.427	**1509**[1]	2.568	**1837**[1]	2.470
1644	2.338	**(1607)**[1]	2.273	**1435**[1]	2.477	1641	2.311
1768[1]	2.113	1459	2.230	**(1431)**[1,2]	2.437	**1480**[1]	2.261
(1447)[1]	2.090	1705	2.225	**(1508)**[1,2]	2.436	1962	2.085
1480[1]	2.072	**1614**[1]	2.139	**(1450)**[1]	2.366		
1941	2.013	**(1891)**[1,2,3]	2.138	**1770**[1]	2.310		
(1884)[1]	2.001	**1696**[1,4]	2.090	1432	2.190		
		(1708)[1]	2.009	**(1506)**[1]	2.162		
				(1467)[1]	2.131		
				1507	2.028		

Dry year references: [1]Borisenkov and Pasetsky (1988, 2003), [2]Kahan (1968), [3]Schubert et al (2014)

Wet year references: [1]Borisenkov and Pasetsky (1988, 2003), [4]Neumann and Lindgren (1979)

827 **Figures:**

828

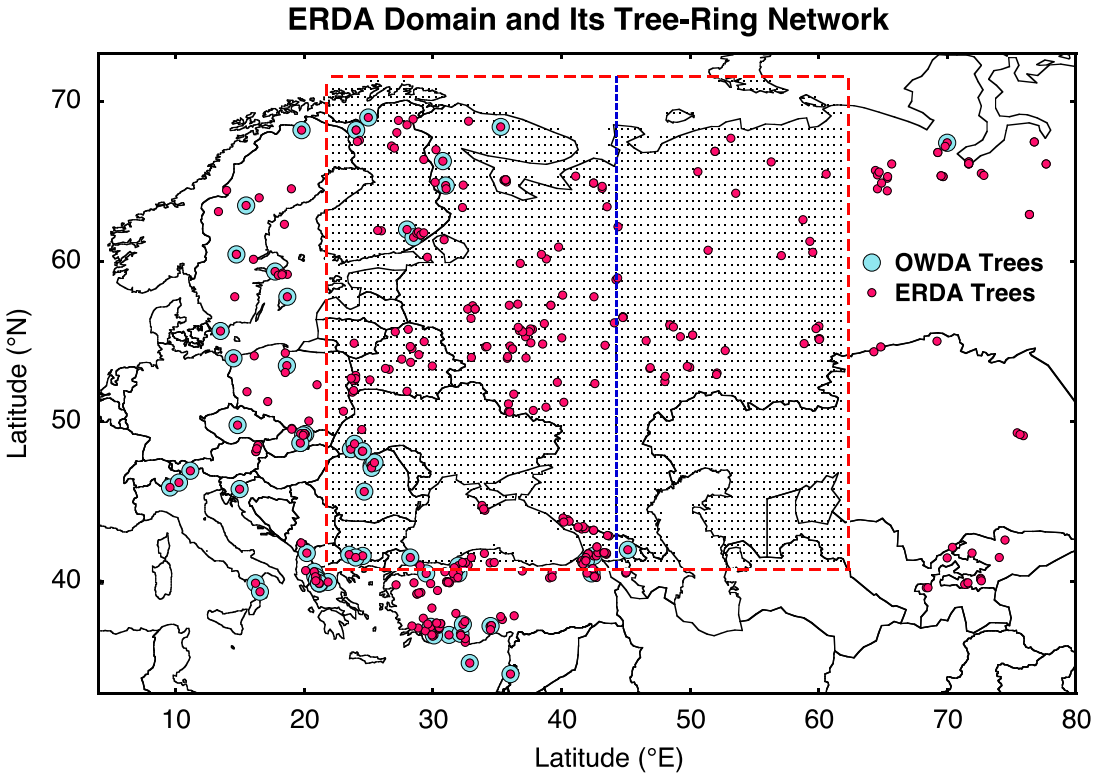

829

830 Figure 1. Map of the European Russia Drought Atlas (ERDA) domain circumscribed by the red
831 dashed rectangle: 4,259 one-half degree grid points of JJA scPDSI. The network of tree-ring
832 chronologies used in the ERDA are shown by small red dots and those used in the OWDA as large
833 blue dots. The vertical blue dashed line is the western limit of the Old World Drought Atlas, which
834 illustrates the inadequate spatial coverage of that domain over European Russia.

835

836

837

838

839

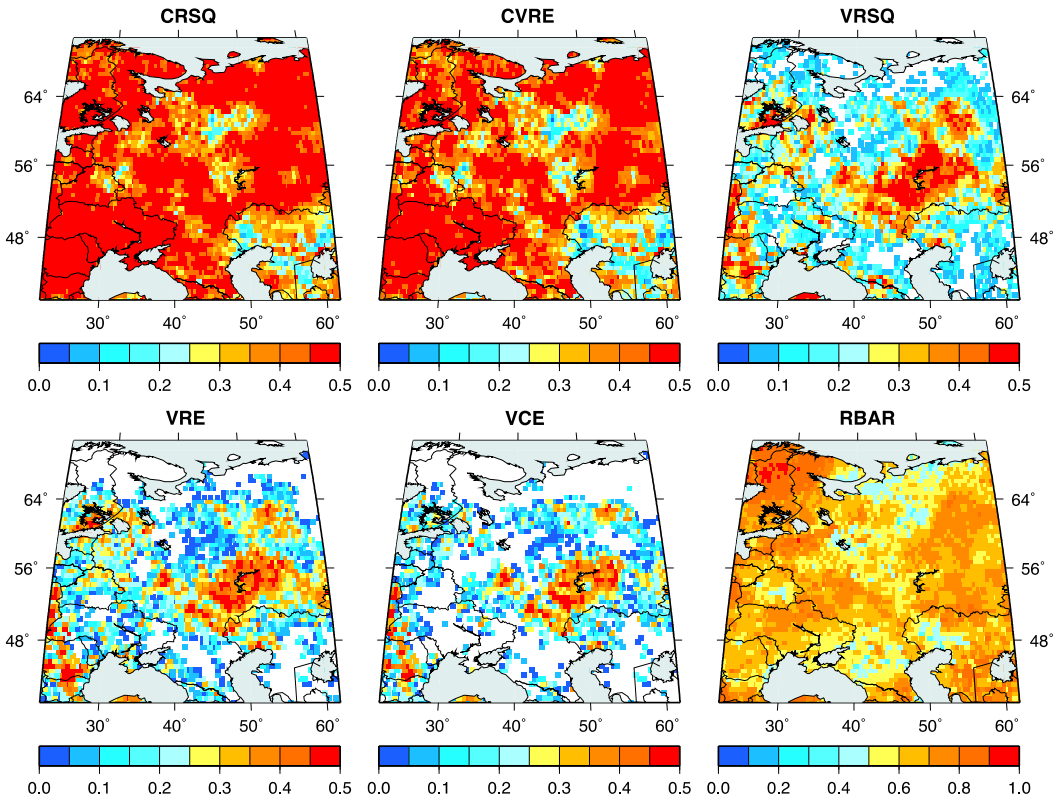

Figure 2. Calibration and validation maps for the ERDA based on an ensemble average of 16 PPR runs as described. CRSQ: calibration period R^2; CVRE: calibration period leave-one-out cross-validation; VRSQ: validation period square of the Pearson correlation; VRE: validation period reduction of error; VCE: validation period coefficient of efficiency; RBAR: average correlation (RBAR) between the 16 ensemble members.

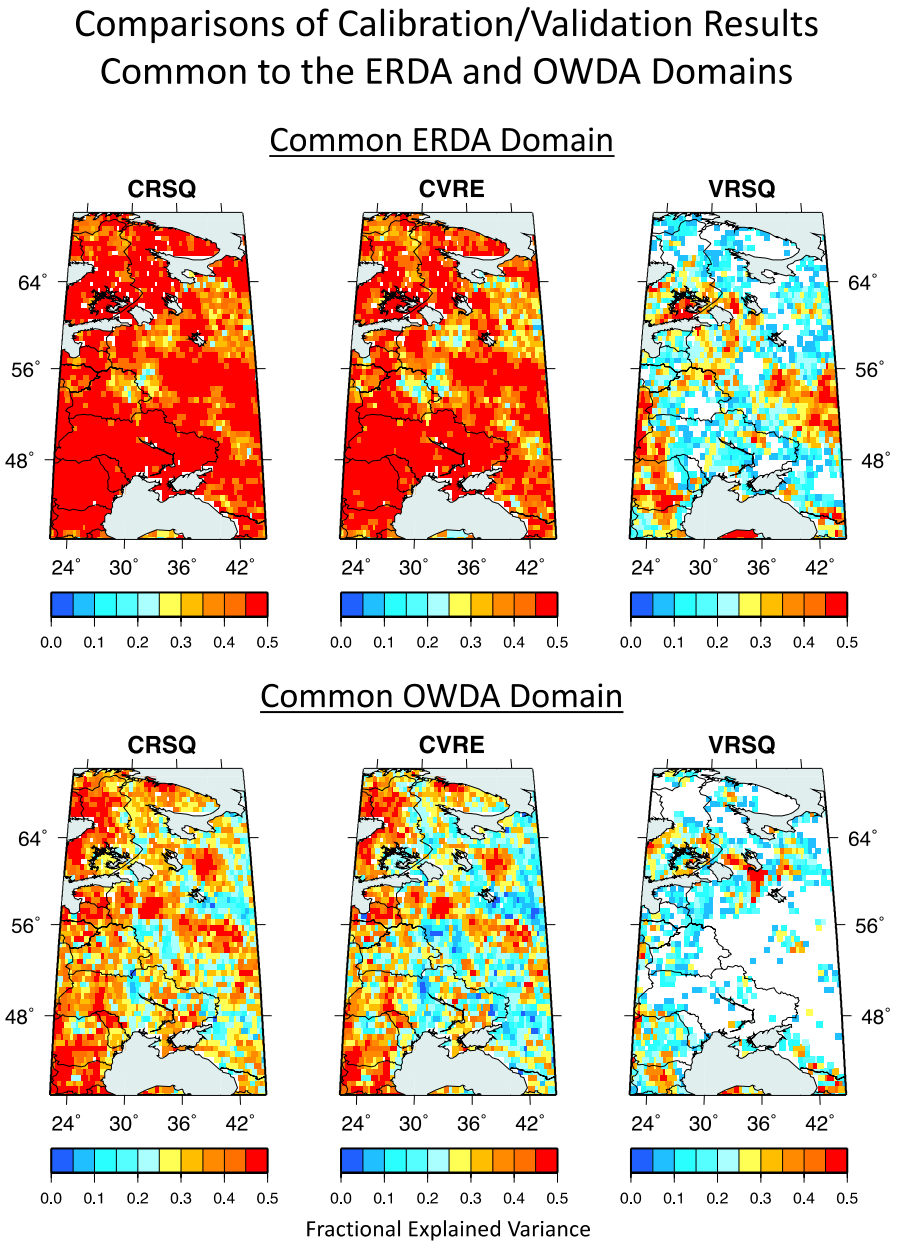

Figure 3. Comparisons of calibration/validation statistics in the domain area common to the ERDA and OWDA. See Fig. 1 for the location of that area to the left (west) of the dashed vertical blue line. Two calibration (CRSQ and CVRE) and one validation (VRSQ) for each are shown. The differences in both calibration and validation are very clear. The ERDA has clearly better skill due to its vastly improved tree-ring network.

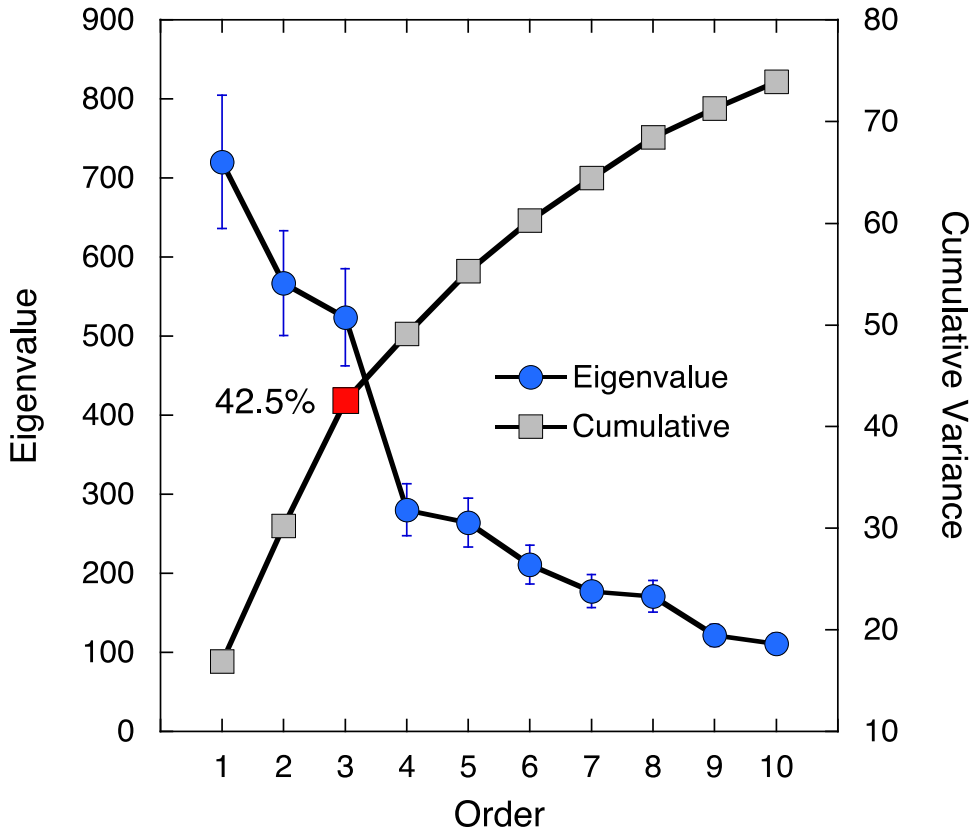

Figure 4. The eigenvalue trace of the ERDA (1400-1983) plotted out to order 10, and the cumulative variance accounted for by those first 10 unrotated EOFs. The uncertainties in the eigenvalues are expressed as ±2 standard errors (vertical bars) based on the standard error estimate from North et al (1982). The first three eigenvalues separate cleanly from the rest and account for 42.5% of total variance, thus determining the eigenvalue cutoff (red square) for Varimax rotation.

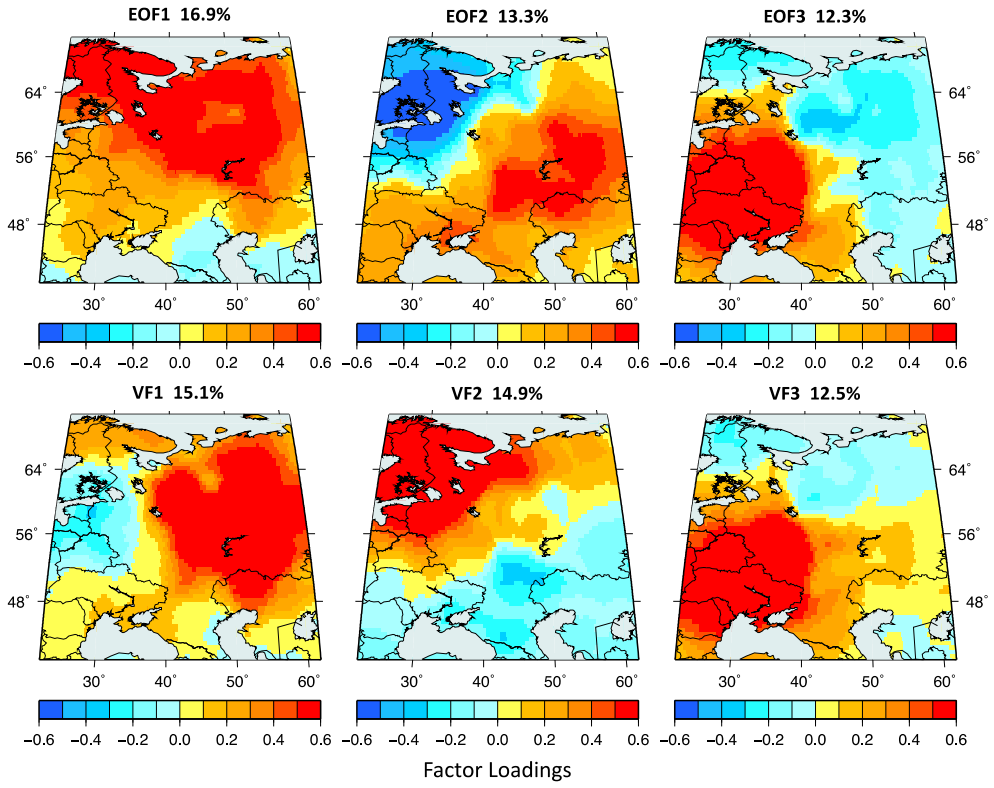

Figure 5. The first three unrotated (EOF) and Varimax rotated (VF) factors, with the variance accounted for by each factor indicated. There is little difference in the variance accounted for before and after rotation, and the total variance (42.5%) is exactly conserved after rotation, but the regional expressions of drought are more cleanly separated after Varimax rotation.

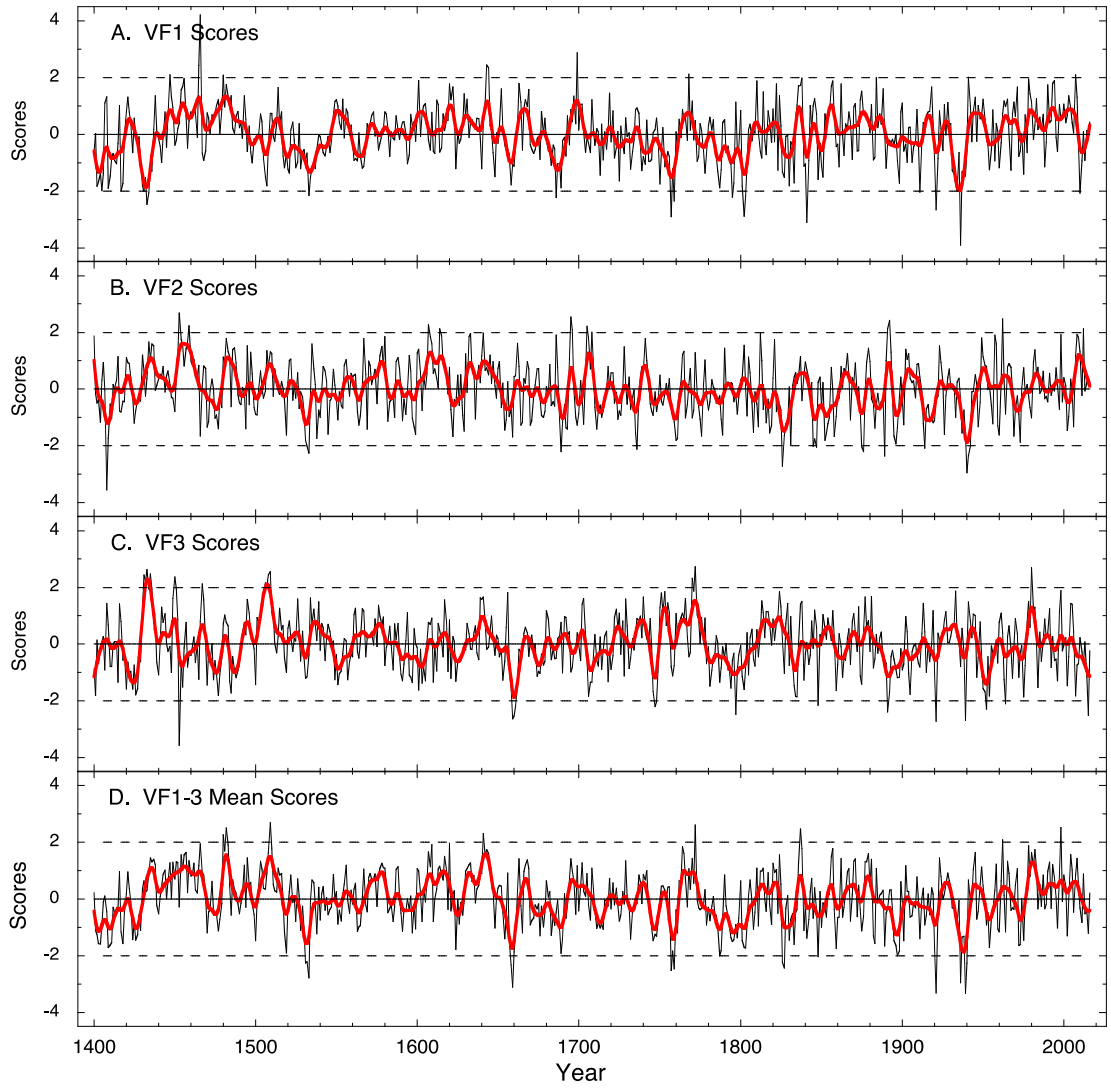

Figure 6. Plots of the ERDA Varimax factor scores (VF1-3) corresponding to the factor patterns shown in Fig. 5. In addition, the mean of the three highlights occurrences of pan-ERDA dry and wet years. Each series is shown in units of standard deviation with a 10-yr low-pass filter (red) applied to each. The horizontal dashed lines are the ±2 standard deviation limits used for identifying years of extreme drought and wetness.

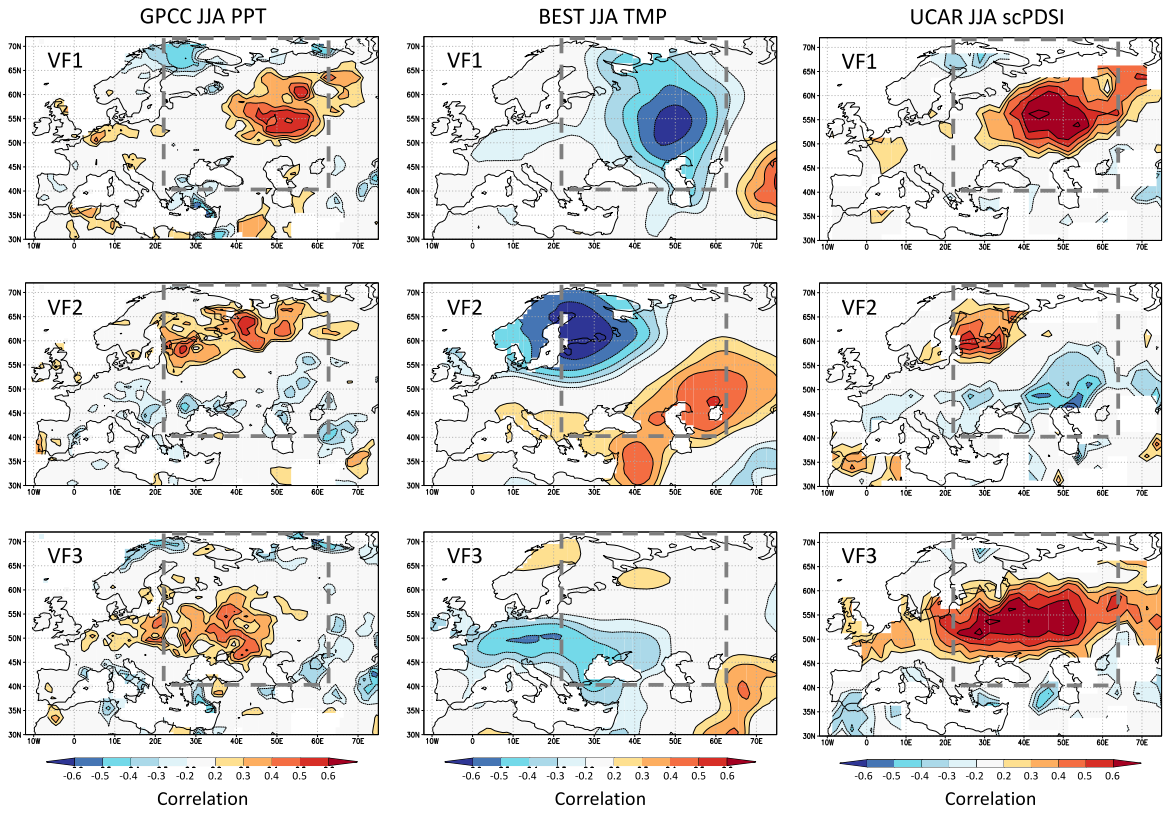

Figure 7. Correlations between the Varimax factors (VF1-VF3) and GPCC precipitation, BEST temperature, and UCAR scPDSI data for the same JJA season based on 1891-1983 data. See the text for details on these climate datasets. Correlations >|0.4| are significant at the 99% confidence level. The rectangle shown in each map delineates the boundaries of the ERDA. The maps are courtesy of KNMI Climate Explorer (van Oldenborgh and Burgers 2005; http://climexp.knmi.nl/).

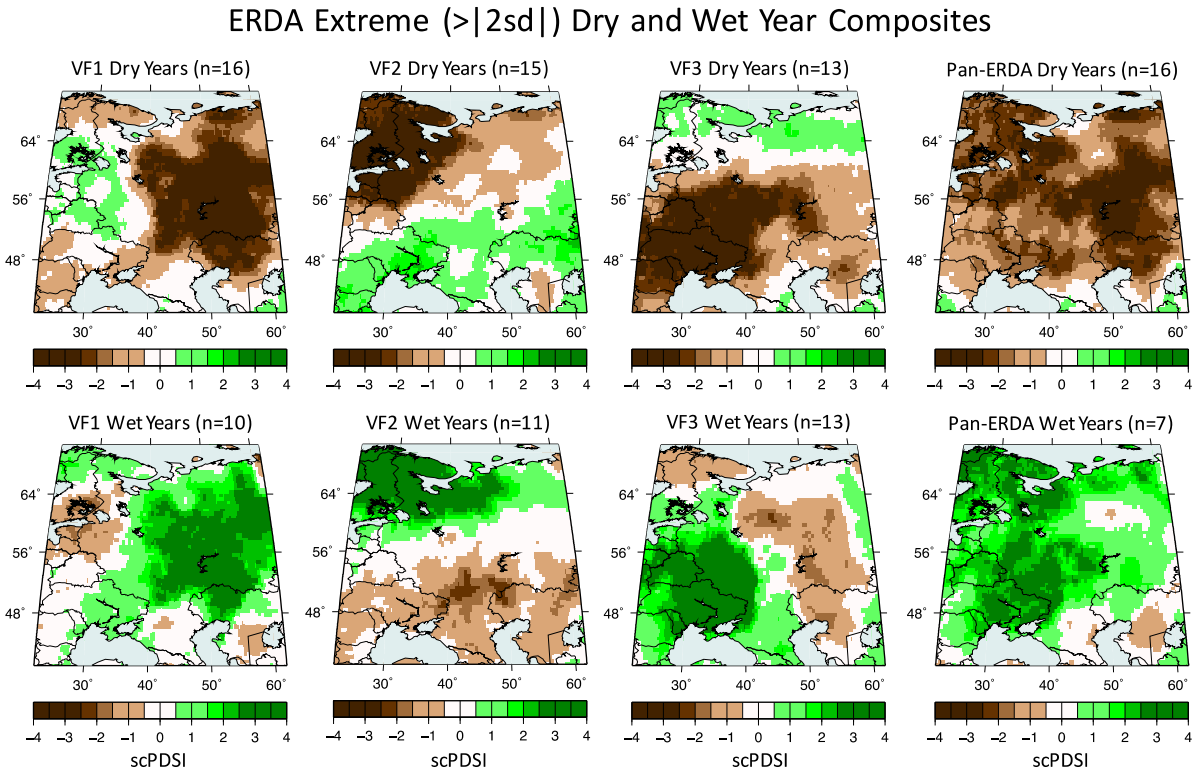

Figure 8. ERDA extreme (>±2sd) dry and wet year composites with the number of years in each composite indicated. The composites are based on the exceedance years indicated in Fig. 6 and listed in Table 1.

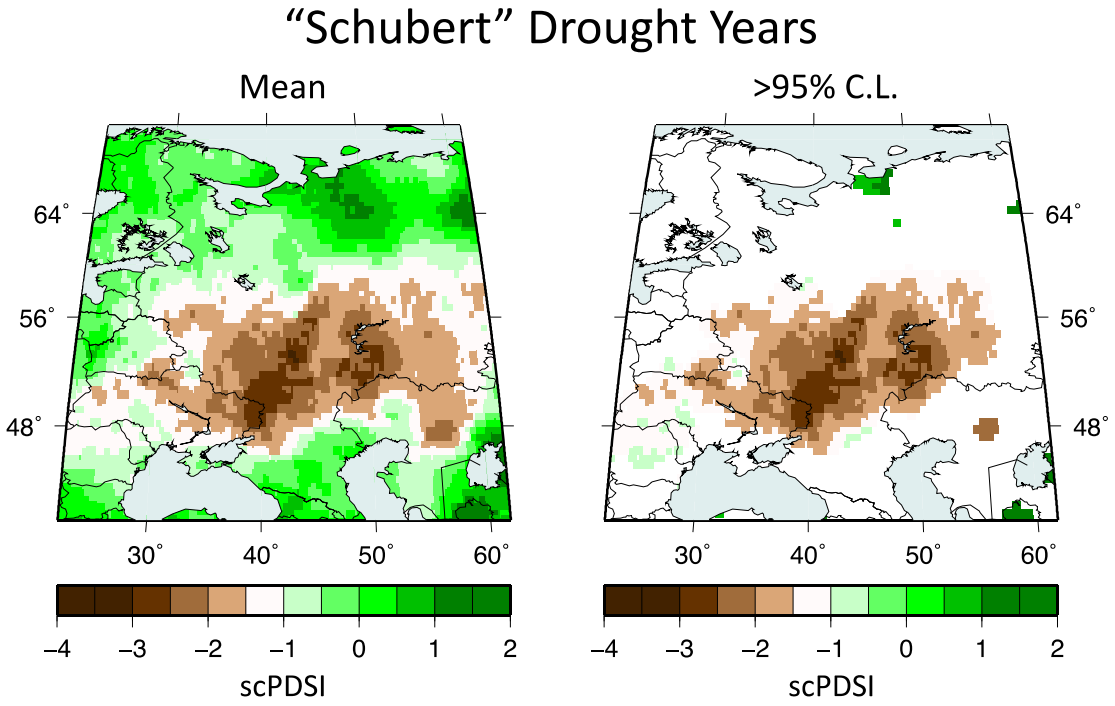

Figure 9. The ten-year composite of years of major historical droughts (lefthand map) extracted from the ERDA, based on the Table B1 list provided by Schubert et al (2014), and where the regional mean is statistically significant ($p<0.05$, 2-tailed; righthand map). The drought years composited from the ERDA are 1875, 1891, 1892, 1897, 1901, 1906, 1911, 1920, 1921, and 1924. All selected years purposely predate the calibration period of the ERDA to avoid fitting bias.

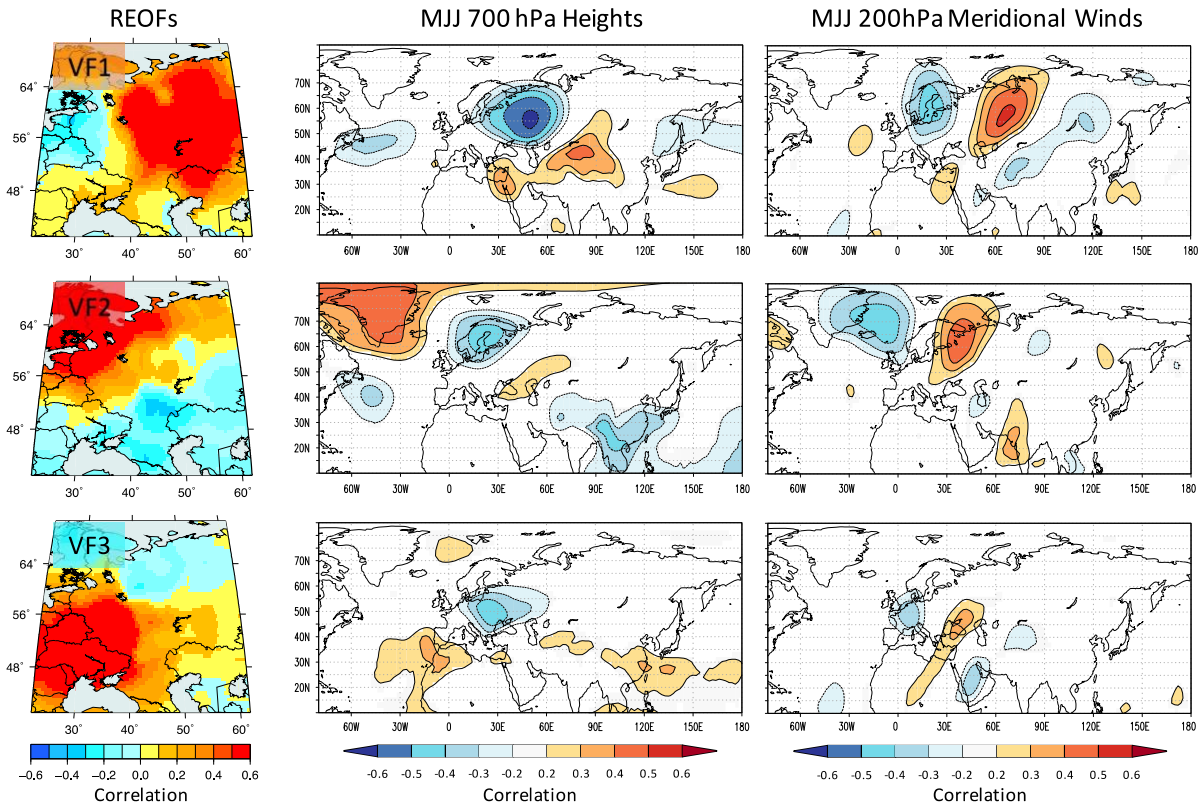

Figure 10. Correlations between the ERDA Varimax factors (VF1-3) and May-June-July (MJJ) average 700 hPa heights and 200 hPa meridional winds from the 20th Century Reanalysis. The analysis period is 1880-1983 and the correlations are based on first-differenced data. The maps are courtesy of KNMI Climate Explorer (van Oldenborgh and Burgers, 2005; http://climexp.knmi.nl/).

Figure1

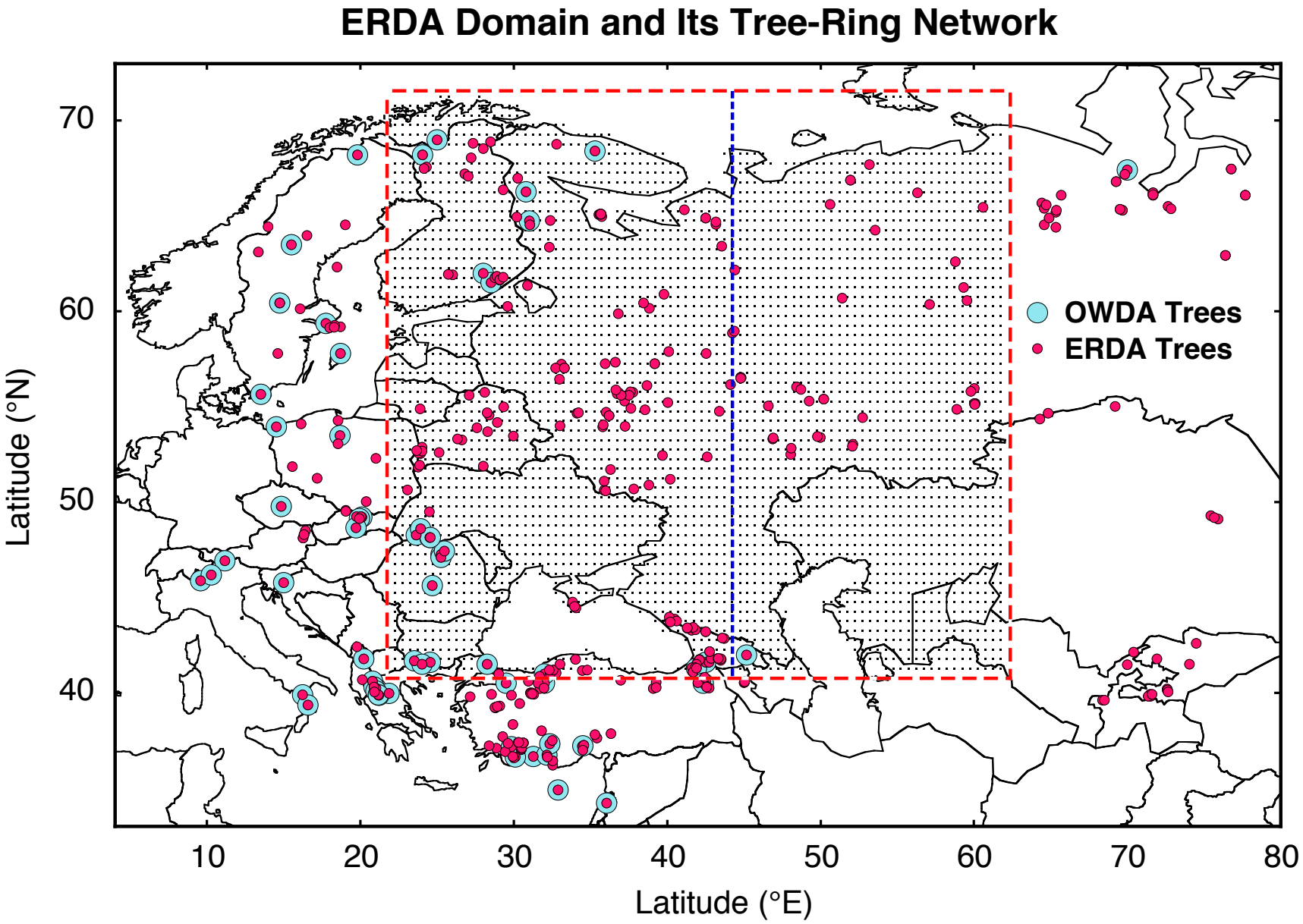
ERDA Domain and Its Tree-Ring Network
OWDA Trees
ERDA Trees
Latitude (°N)
Latitude (°E)
70
60
50
40
10
20
30
40
50
60
70
80

Figure2

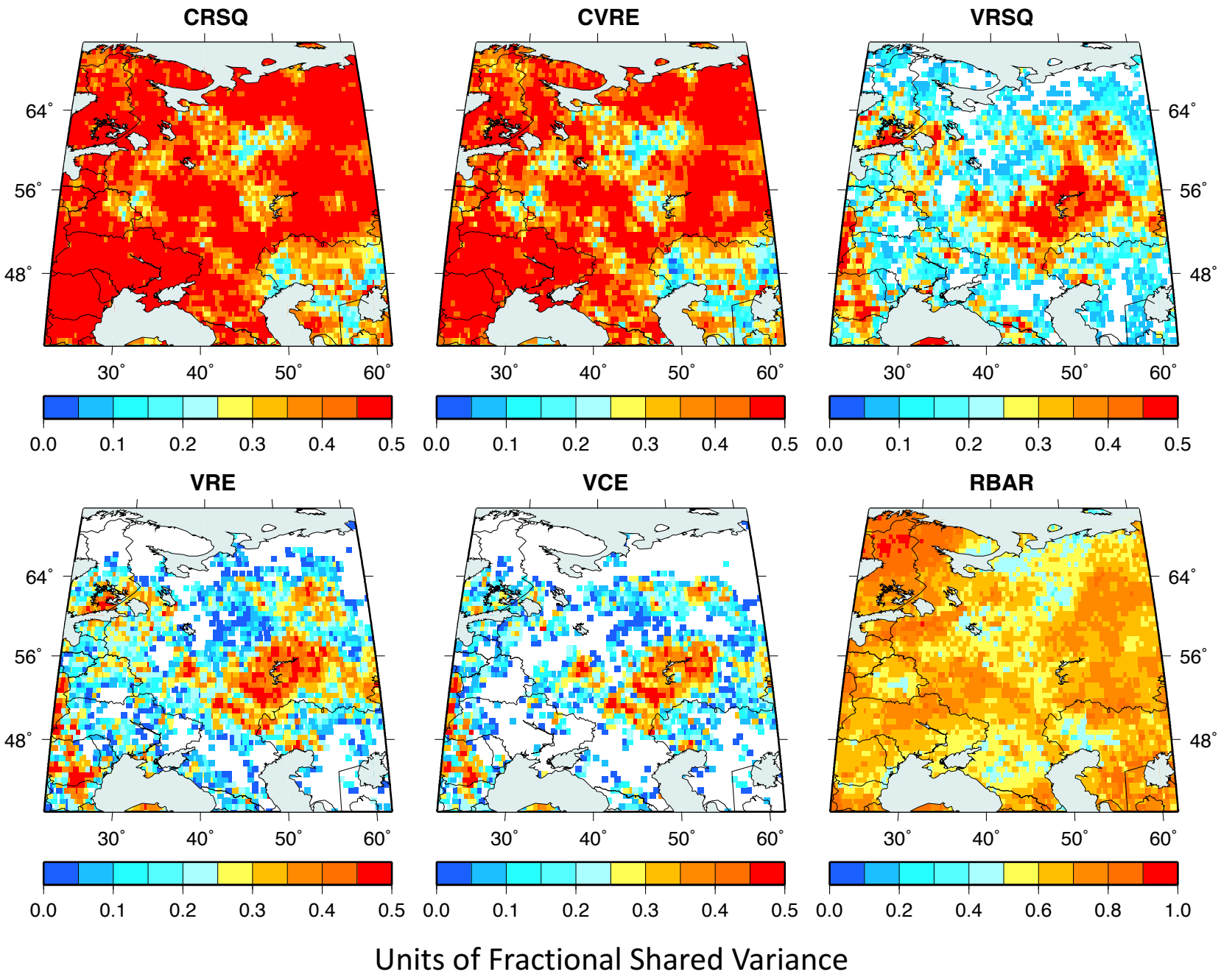
CRSQ
CVRE
VRSQ
VRE
VCE
RBAR
64˚
56˚
48˚
30˚
40˚
50˚
60˚
0.0
0.1
0.2
0.3
0.4
0.5
0.6
0.8
1.0
Units of Fractional Shared Variance

Figure3

Comparisons of Calibration/Validation Results Common to the ERDA and OWDA Domains

Common ERDA Domain

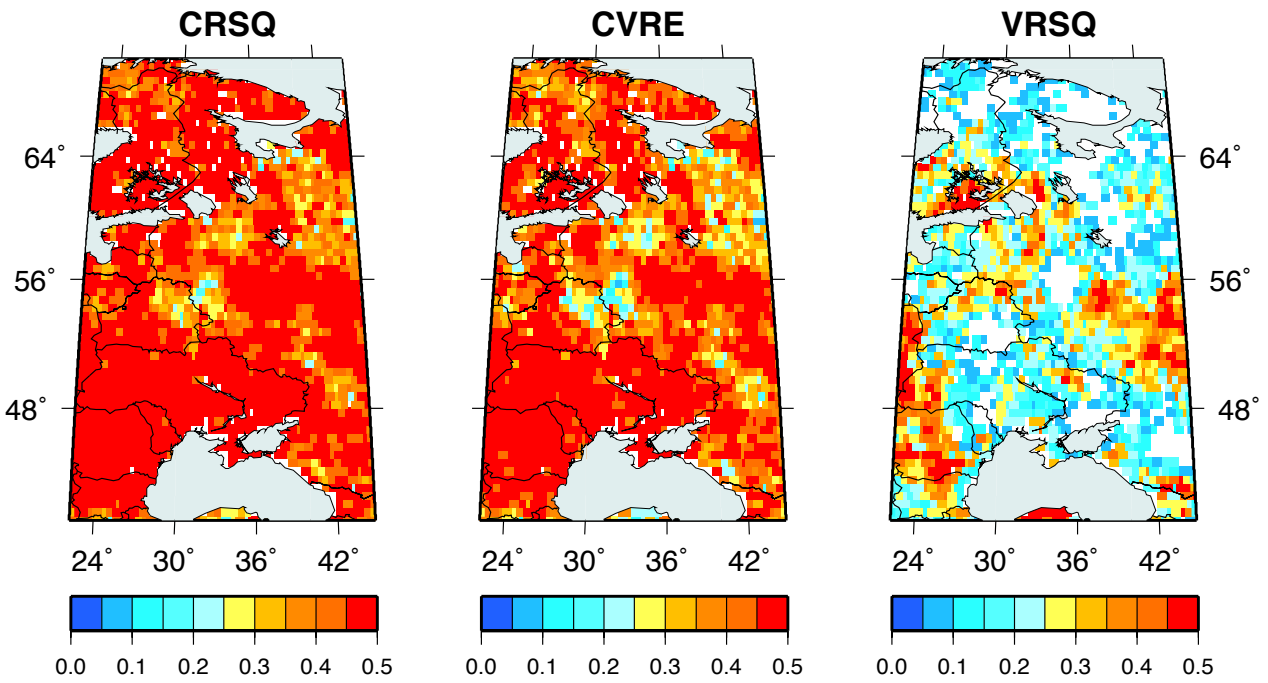

Common OWDA Domain

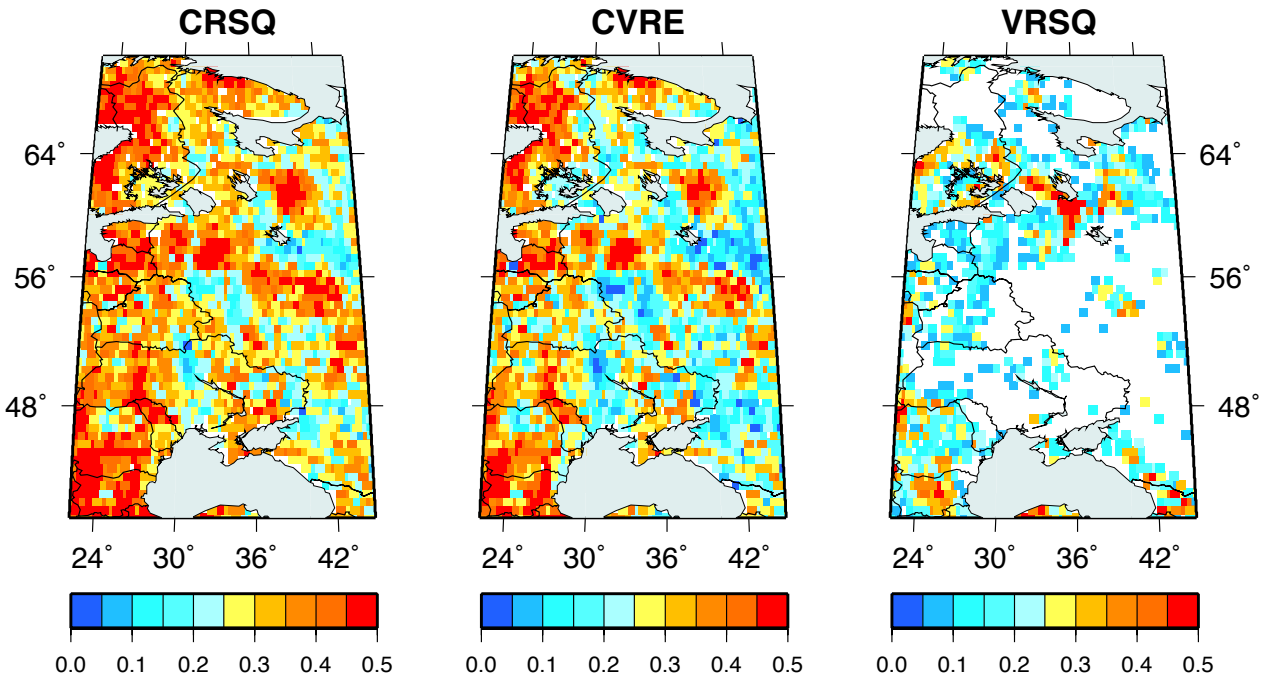

Fractional Explained Variance

Figure4

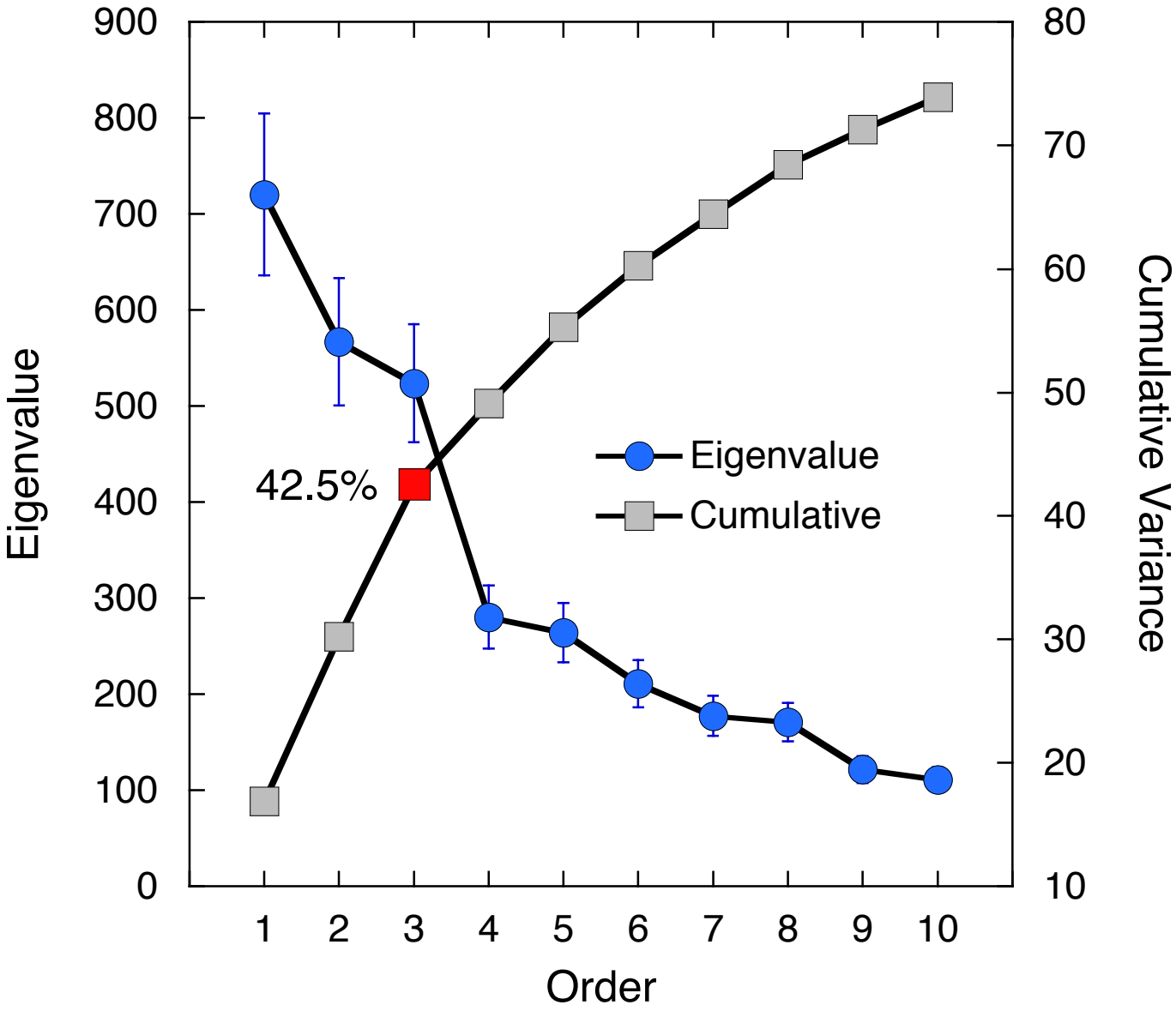
900
800
700
600
500
400
300
200
100
0
Eigenvalue
80
70
60
50
40
30
20
10
Cumulative Variance
1
2
3
4
5
6
7
8
9
10
Order
42.5%
Eigenvalue
Cumulative

Figure5

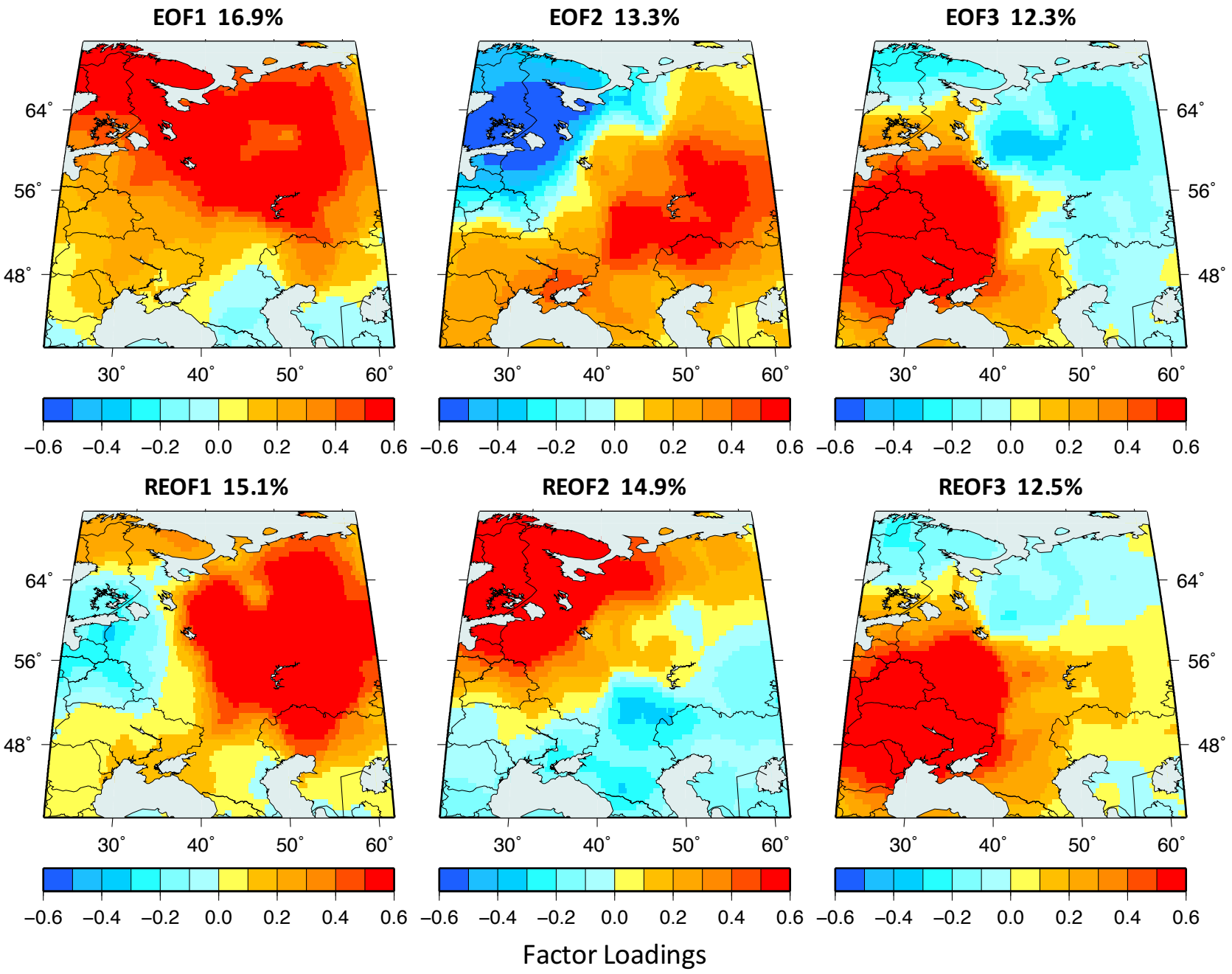
EOF1 16.9%
EOF2 13.3%
EOF3 12.3%
REOF1 15.1%
REOF2 14.9%
REOF3 12.5%
64˚
56˚
48˚
30˚
40˚
50˚
60˚
−0.6 −0.4 −0.2 0.0 0.2 0.4 0.6
Factor Loadings

Figure6

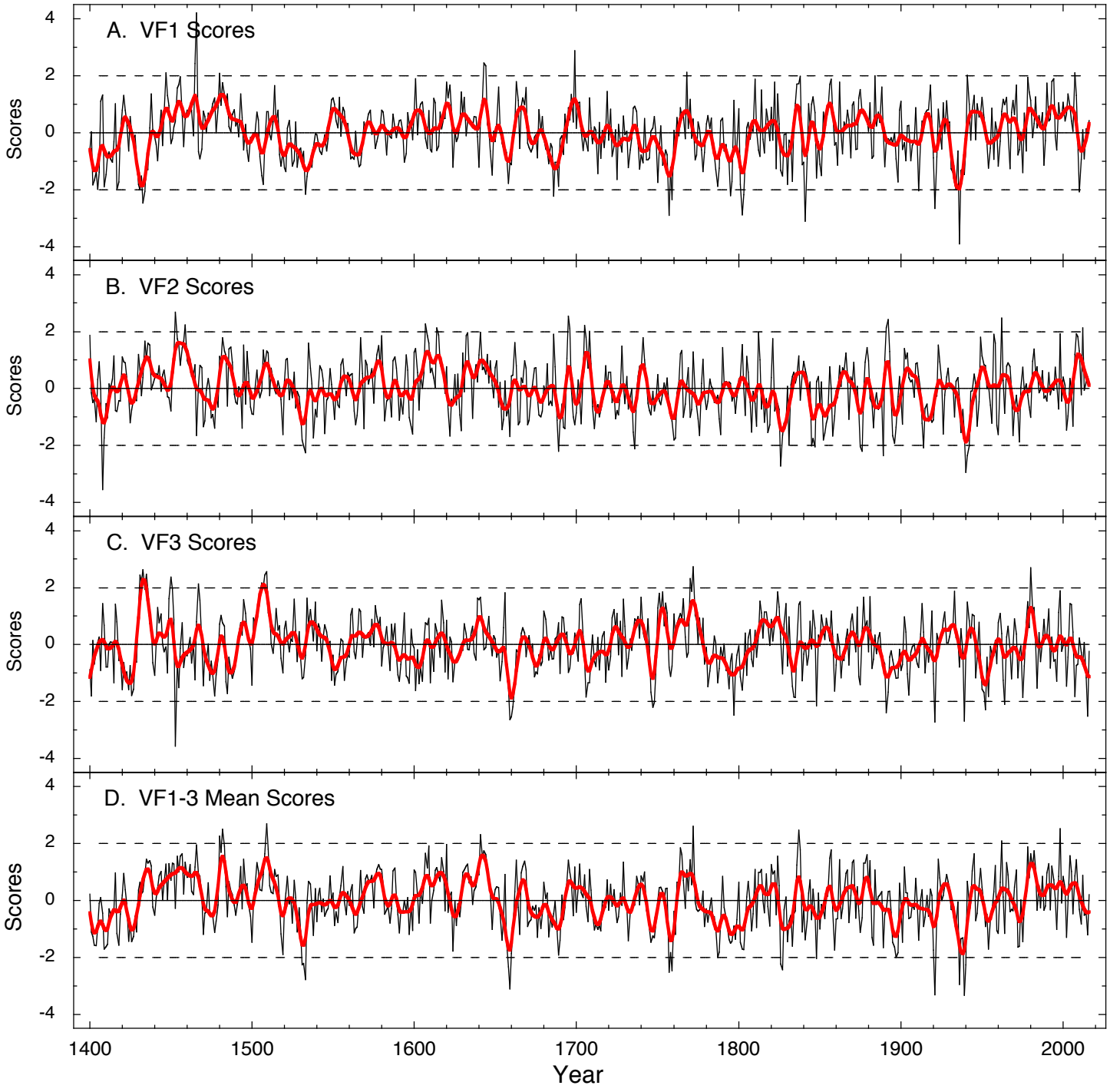
A. VF1 Scores
B. VF2 Scores
C. VF3 Scores
D. VF1-3 Mean Scores
Scores
4
2
0
-2
-4
1400
1500
1600
1700
1800
1900
2000
Year

Figure7

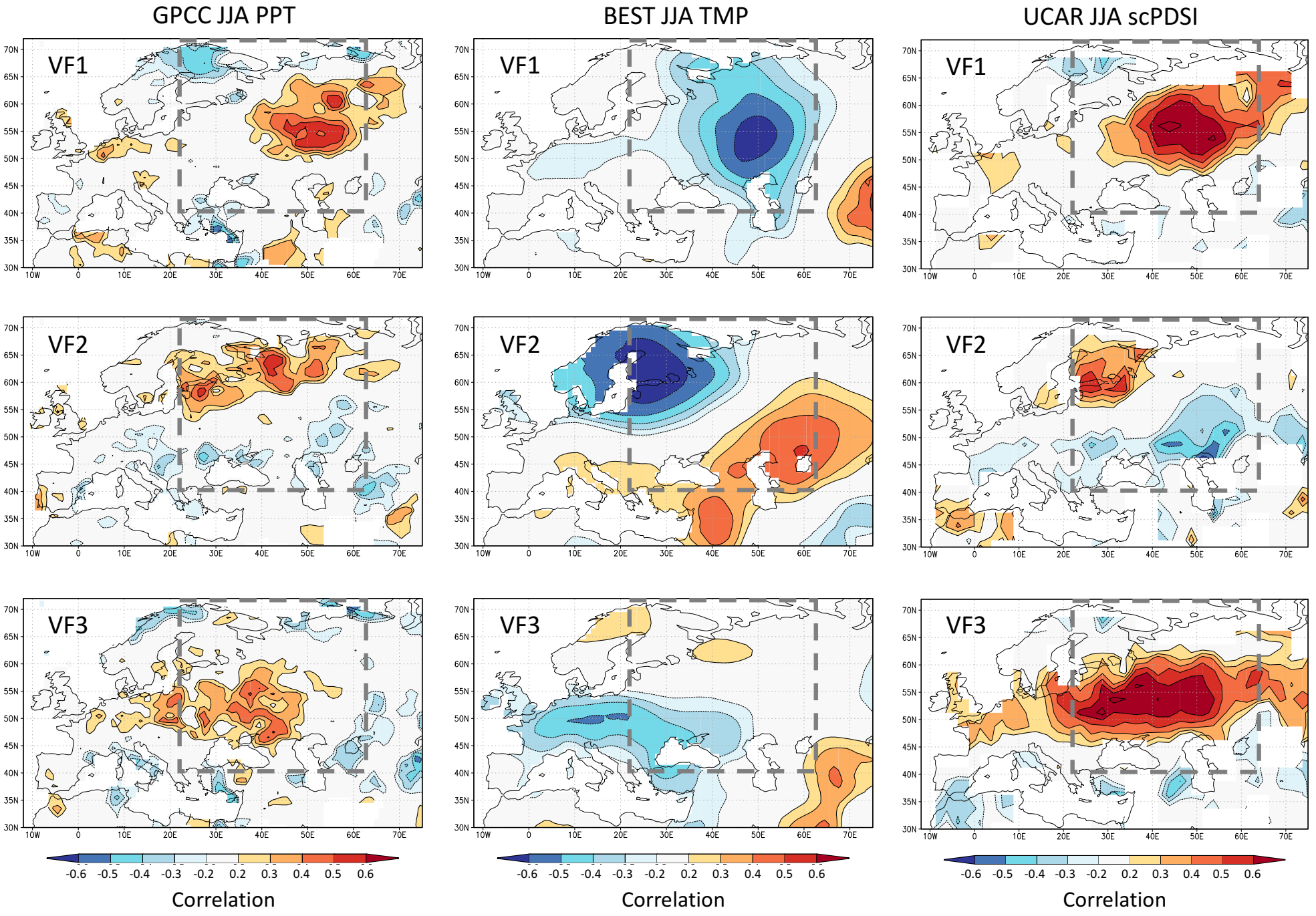
GPCC JJA PPT
BEST JJA TMP
UCAR JJA scPDSI
VF1
VF2
VF3
70N
65N
60N
55N
50N
45N
40N
35N
30N
10W
0
10E
20E
30E
40E
50E
60E
70E
-0.6 -0.5 -0.4 -0.3 -0.2 0.2 0.3 0.4 0.5 0.6
Correlation

Figure8

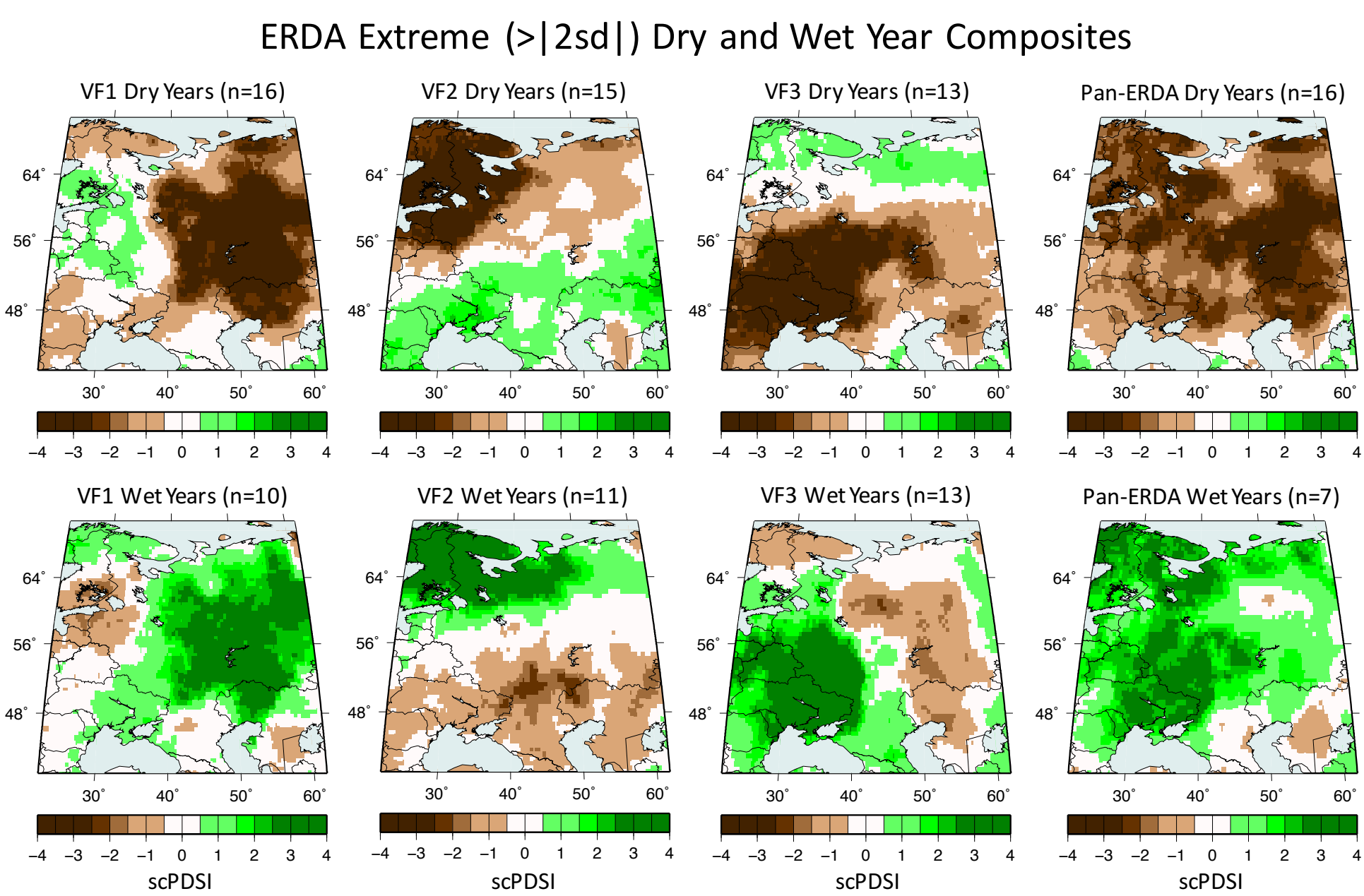
ERDA Extreme (>|2sd|) Dry and Wet Year Composites
VF1 Dry Years (n=16)
VF2 Dry Years (n=15)
VF3 Dry Years (n=13)
Pan-ERDA Dry Years (n=16)
VF1 Wet Years (n=10)
VF2 Wet Years (n=11)
VF3 Wet Years (n=13)
Pan-ERDA Wet Years (n=7)
64°
56°
48°
30°
40°
50°
60°
−4 −3 −2 −1 0 1 2 3 4
scPDSI

Figure9

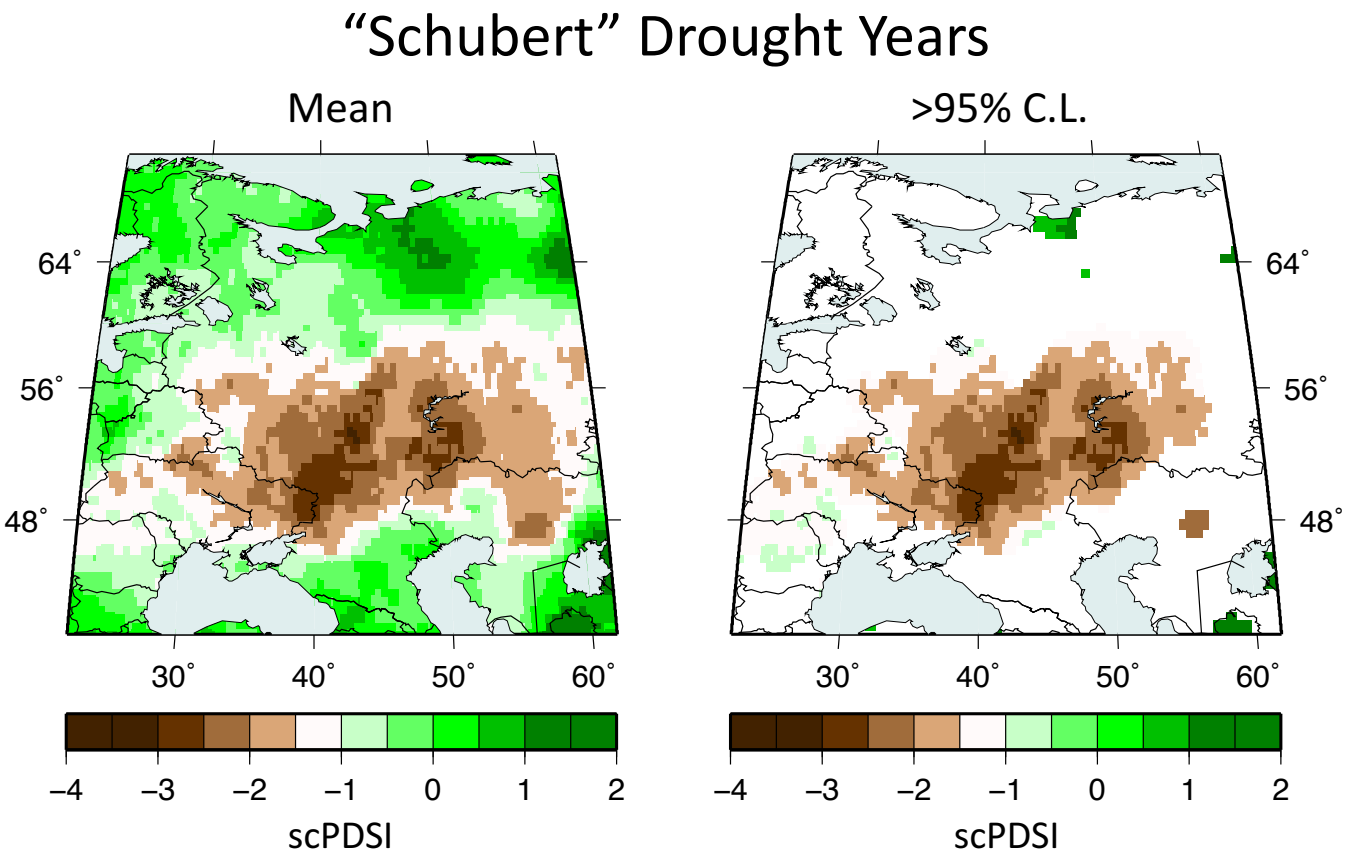
“Schubert” Drought Years
Mean
>95% C.L.
64˚
56˚
48˚
30˚
40˚
50˚
60˚
−4
−3
−2
−1
0
1
2
scPDSI

Figure10

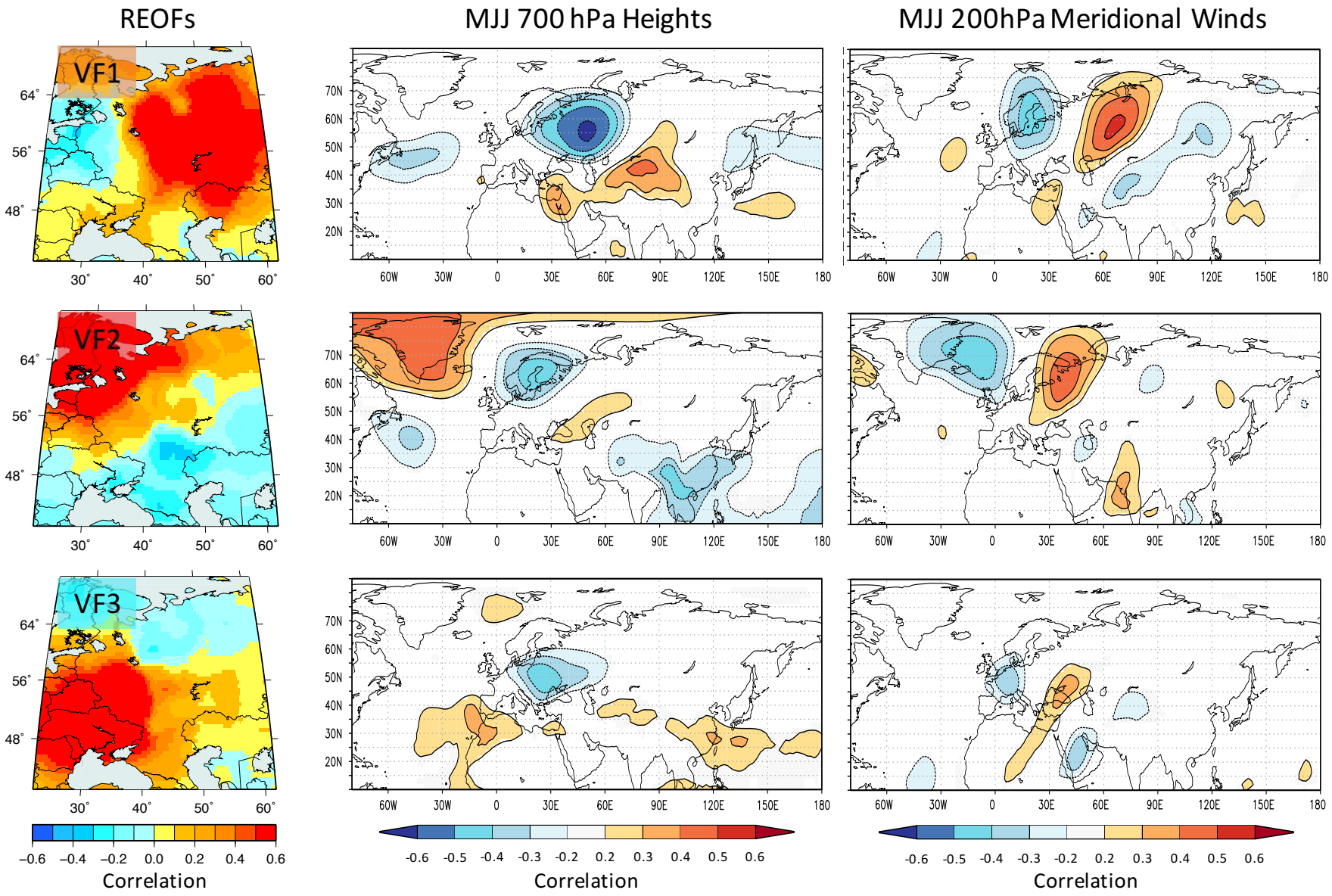
REOFs
MJJ 700 hPa Heights
MJJ 200hPa Meridional Winds
VF1
VF2
VF3
64˚
56˚
48˚
30˚
40˚
50˚
60˚
70N
60N
50N
40N
30N
20N
60W
30W
0
30E
60E
90E
120E
150E
180
−0.6 −0.4 −0.2 0.0 0.2 0.4 0.6
-0.6 -0.5 -0.4 -0.3 -0.2 0.2 0.3 0.4 0.5 0.6
Correlation

Table1

Table 1. Lists of driest and wettest years in the three Varimax factors estimated from the ERDA (1400-1983), plus the mean of those scores, all scaled in units of standard deviation from the mean. The driest and wettest years are selected as those that equal or exceed ±2 standard deviations from the mean. Years with units exceeding ±1.99 standard deviation units are also considered close enough to include in these lists. There are three such exceptions.

FACTOR #1 DRY		FACTOR #2 DRY		FACTOR #3 DRY		MEAN FACTOR DRY	
YEAR	-2SD	YEAR	-2SD	YEAR	-2SD	YEAR	-2SD
1936	-3.897	1408	-3.547	1453	-3.560	1939	-3.336
1841	-3.106	1940	-2.952	1921	-2.717	1921	-3.316
1757	-2.904	1826	-2.721	1939	-2.682	1659	-3.109
1802	-2.888	1941	-2.361	1659	-2.624	1936	-2.949
1921	-2.661	1889	-2.356	1660	-2.524	1533	-2.777
1433	-2.474	1533	-2.258	1797	-2.481	1757	-2.520
1759	-2.355	1876	-2.206	1891	-2.394	1759	-2.472
1686	-2.219	1689	-2.201	1952	-2.293	1827	-2.430
1795	-2.206	1736	-2.117	1747	-2.206	1658	-2.329
1803	-2.175	1914	-2.078	1661	-2.183	1531	-2.266
1533	-2.163	1847	-2.042	1848	-2.151	1940	-2.258
1434	-2.061	1875	-2.031	1964	-2.110	1826	-2.219
1911	-2.040	1942	-2.003	1748	-2.034	1532	-2.213
1417	-2.000	1845	-2.003			1848	-2.039
1431	-1.999	1532	-2.003			1787	-2.002
1934	-1.991					1897	-1.999
FACTOR #1 WET		**FACTOR #2 WET**		**FACTOR #3 WET**		**MEAN FACTOR WET**	
YEAR	+2SD	YEAR	+2SD	YEAR	+2SD	YEAR	+2SD
1466	4.201	1453	2.684	1772	2.731	1509	2.683
1699	2.877	1695	2.543	1980	2.704	1772	2.602
1643	2.444	1962	2.469	1433	2.627	1482	2.491
1465	2.419	1892	2.427	1509	2.568	1837	2.470
1644	2.338	1607	2.273	1435	2.477	1641	2.311
1768	2.113	1459	2.230	1431	2.437	1480	2.261
1447	2.090	1705	2.225	1508	2.436	1962	2.085
1480	2.072	1614	2.139	1450	2.366		
1941	2.013	1891	2.138	1770	2.310		
1884	2.001	1696	2.090	1432	2.190		
		1708	2.009	1506	2.162		
				1467	2.131		
				1507	2.028		